arXiv:astro-ph/0505504 v3 27 Sep 2005

The Calibration of the *Swift*/UVOT Optical Observations: A Recipe for Photometry

Weidong Li, Saurabh Jha, Alexei V. Filippenko, Joshua S. Bloom, David Pooley, Ryan J. Foley, & Daniel A. Perley

Department of Astronomy, University of California, Berkeley, CA 94720-3411.

email: (wli,sjha,alex,jbloom,dave,rfoley,dperley)@astro.berkeley.edu

Received _____; accepted _____

Submitted to PASP

ABSTRACT

The Ultraviolet-Optical Telescope (UVOT) onboard *Swift* has the capability to provide critical insight into the physics of the early afterglows of gamma-ray bursts (GRBs). But without precise calibration of the UVOT to standard photometric systems, it is impossible to leverage late-time, ground-based follow-up data to the early-time UVOT observations. In this paper, we present a calibration of the *Swift*/UVOT photometry to the standard Johnson UBV system for the UVOT U, B, and V filters, and a step-by-step photometry recipe for analyzing these data. We base our analysis on aperture photometry performed on the ground-based and UVOT observations of the local standard stars in the fields of supernovae (SNe) 2005am and 2005cf, and a number of Landolt standard stars. We find that the optimal photometry aperture radius for UVOT data is small (2″.5 for unbinned data, 3″.0 for 2×2 binned data), and show that the coincidence-loss (C-loss) correction is important even for relatively faint magnitudes (mag 16 to 19). Based on a theoretically motivated model, we fit the C-loss correction with two parameters, the photometric zero point (ZP) and the saturation magnitude (m_∞), and derive tight constraints for both parameters [$\sigma(ZP) = 0.01$ mag and $\sigma(m_\infty) = 0.02$ mag)]. We find that the color term correction is not necessary for the UVOT B and V filters, but is necessary for the U filter for blue objects [$(U - V) < 0.4$ mag]. We analyze the UVOT UBV photometry of SN 2005am, and find that the UVOT photometry is generally consistent with the ground-based observations, but a difference of up to 0.5 mag is found when the SN became faint. We also apply our calibration results to the UVOT observations of GRB 050603. There is a scatter of ∼0.04–0.08 mag in our final UVOT photometry, the cause of which is unclear, but may be partly due to the spatial variation in the pixel sensitivity of

the UVOT detector.

Subject headings: gamma-rays: bursts – space vehicles: instruments – ultraviolet: general – techniques: photometric

1. Introduction

The successful launch and operation of *Swift* heralds a new era for the study of gamma-ray bursts (GRBs) and related phenomena. *Swift*, a multi-wavelength space observatory, has three instruments: the Burst Alert Telescope (BAT; Barthelmy et al. 2005), the X-ray Telescope (XRT; Burrows et al. 2005), and the UV/Optical Telescope (UVOT; Roming et al. 2005). Together these instruments observe GRBs and their afterglows in the gamma-ray, X-ray, and ultraviolet/optical wavebands, respectively.

Compared to previous space missions dedicated to the study of GRBs, the UVOT is unique to *Swift*, although it is identical to the Optical Monitor on *XMM-Newton* (Mason et al. 2001). The UVOT is a 30 cm Ritchey-Chrétien reflector, using micro-channel intensified CCDs as detectors. These are photon-counting devices capable of detecting very low signal levels. The UVOT is designed to rapidly respond to localizations of GRBs by the BAT and XRT instruments. It has UV capability which is not possible from the ground, and it is also more sensitive than most ground-based rapid-response telescopes. From the UVOT images, optical afterglows of GRBs can be quickly identified and studied, which helps to optimize ground-based observations and provides information on the early-time photometric evolution of these GRB afterglows.

It is expected that the early UVOT observations will be used in conjunction with subsequent ground-based images. It is thus essential that the UVOT and the ground-based images are calibrated on the same photometric system. In the optical bands, the most frequently used ground-based photometric system is the Johnson/Cousins *UBVRI* system, and the *Swift* calibration database (CALDB) webpage [1] provides calibration files for the various UVOT filters. Table 1 lists these calibration results from the latest release (2005

[1]http://heasarc.gsfc.nasa.gov/docs/heasarc/caldb/swift

Aug. 12). We note that the uncertainties for the zero points are relatively large (0.1 – 0.2 mag) for most filters.

Since it is important to tie the UVOT photometry with that obtained from the ground, in this paper we present an independent study of the photometric calibrations for the UVOT filters, in particular in the U, B, and V bands. This calibration is derived from observations of two supernovae, SN 2005am and SN 2005cf (but only the light curve of SN 2005am is presented in this paper), and Landolt (1992) standard stars in the *Swift* quicklook database. The other goal of this paper is to analyze the UVOT observations with tools that are familiar to optical astronomers, such as IRAF and DoPhot, and search for optimal parameters for doing proper photometry. The NASA High Energy Astrophysics Science Archive Research Center (HEASARC)[2] has supplied software tools to analyze data from all *Swift* instruments. For UVOT images, these tools suggest aperture photometry using Sextractor (Bertin & Arnouts 1996).

The ground-based observations and reduction of SN 2005am are described in §2, and photometric calibration analyses are presented in §3. Section §4 discusses the UVOT photometry of SN 2005am and compares this to the ground-based observations. We apply our calibration results and optimal photometric parameters to the UVOT observations of GRB 050603 in §5. The discussions are presented in §6 and the conclusions are summarized in §7.

2. Analysis of the Ground-based Observations of SN 2005am

SN 2005am was discovered by R. Martin (Martin, Yamaoka, & Itagaki 2005) on 2005 Feb. 22 (UT dates are used throughout this paper) during the course of the Perth

[2]http://heasarc.gsfc.nasa.gov/ .

Automated SN Search. It was classified as a Type Ia SN (SN Ia) by Modjaz et al. (2005a) from a spectrum taken with the F. L. Whipple Observatory 1.5-m telescope. After some delays caused by bad weather, we began to follow the SN with the robotic 0.76-m Katzman Automatic Imaging Telescope (KAIT; see Li et al. 2000; Filippenko et al. 2001; Filippenko 2003) at Lick Observatory on Mar. 6. Several epochs of observations were also obtained with the 1-m Nickel telescope at Lick Observatory.

Photometric calibrations of the SN 2005am field were performed under photometric conditions on 4 nights: Mar. 9 and 13 with KAIT, and Mar. 12 and 14 with the Nickel telescope. During each photometric night, many Landolt (1992) standard-star sequences (9–12 for Nickel, 16–18 for KAIT) were observed at a range of airmasses. Instrumental magnitudes for the standard stars were measured using aperture photometry with the IRAF[3] DAOPHOT package (Stetson 1987) and then employed to determine transformation coefficients to the standard Johnson-Cousins *BVRI* system. The derived transformation coefficients and color terms were then used to calibrate a sequence of local standard stars in the field of SN 2005am (hereafter SN 2005am field stars). Figure 1 shows a finder chart for the SN 2005am field, while Table 2 lists the magnitudes of the local standard stars and the root-mean-square (RMS) of the magnitude measurements in all the photometric nights. Notice that the local standard stars have different numbers of calibrations because the two telescopes have different total fields of view. The majority of the calibrated magnitudes have uncertainties smaller than 0.03 mag.

Also listed in Table 2 are preliminary *U*-band calibrations for some of the bright stars in the SN 2005am field. This calibration was done on Apr. 6 under photometric

[3]IRAF (Image Reduction and Analysis Facility) is distributed by the National Optical Astronomy Observatories, which are operated by the Association of Universities for Research in Astronomy, Inc., under cooperative agreement with the National Science Foundation.

conditions with KAIT, but only one *UBVRI* sequence of the Landolt field "Rubin 152" was observed at the same airmass as when SN 2005am was imaged. Inspection of the data also reveals that the measured *BVRI* magnitudes for the SN 2005am field stars from this particular night are offset from the calibration listed in Table 2 by a constant 0.20±0.01 mag. Further investigation suggests that the dome was slightly blocking the telescope when the standard-star field was imaged due to a dome position zero-point error. We thus shift the calibrated U-band magnitudes by the same amount. We set an uncertainty of 0.05 mag to the calibrated U-band magnitudes, but because we had only one standard-star sequence, and we had to apply an arbitrary shift to the measured magnitudes, the real uncertainty could be as high as 0.10 mag. As a result, we caution that the results derived from the U-band calibration of the SN 2005am field should be regarded as preliminary. In section § 3.3, we present a better U-band calibration for the field of SN 2005cf. Those data, combined with U-band observations of Landolt standard stars (also in § 3.3), lead to the final U-band calibration (§ 3.4).

As can be seen in Figure 1, SN 2005am occurred in the outskirts of its host galaxy, and is separated from a relatively bright foreground star by only 7″. To derive proper photometry for SN 2005am, we use the point-spread-function (PSF) fitting method (Stetson 1987) in the IRAF/DAOPHOT package to perform differential photometry of SN 2005am relative to the local standard stars; see Li et al. (2003a) for more details. Color terms for the KAIT and the Nickel filters have been well established from photometric calibrations of over 20 photometric nights at each telescope, and have been applied to derive the final photometry for SN 2005am as listed in Table 3. The quoted uncertainty of the magnitudes is a quadrature sum of the PSF-fitting photometry and the transformation scatter from the local standard stars. Although SN 2005am has a complex background, the final photometry has an overall uncertainty of only 0.03–0.04 mag because the SN is significantly brighter than the background, and there are plenty of bright isolated stars in the field from which to

construct a robust PSF for the images.

The derived light curve of SN 2005am is shown in Figure 2, together with fits using the Multicolor Light Curve Shape (MLCS2k2) method (Jha 2002; Jha, Riess, &Kirshner 2006), which is an empirical method to model the light curves of a SN Ia to derive its luminosity distance. Overall, the KAIT and the Nickel photometry are consistent with each other (except perhaps the two I-band data points near JD 2453470). SN 2005am shows a photometric evolution rather typical of a SN Ia: a second peak in the I band, a shoulder in the R band, and a smooth decline after maximum in the bluer bands. Our follow-up observations began near the maximum of the B band, and 2–3 days before maximum in the other bands. The MLCS2k2 fits are typical for a well-observed SN Ia. SN 2005am is not significantly reddened by dust in its host galaxy (host $A_V = 0.09 \pm 0.07$ mag). It is also a somewhat rapidly declining and subluminous object (by approximately 0.5 mag), intermediate between normal SNe Ia and the most subluminous objects like SN 1991bg (Filippenko et al. 1992). This makes SN 2005am an important addition to the sample of nearby SNe Ia, with only a handful of similar objects known (Jha et al. 2005).

The SN 2005am field stars as listed in Table 2 are used to study the photometric calibrations of the UVOT filters in §3. We investigate the optimal parameters to do photometry on these stars in the UVOT images, so that the best possible consistency between the ground-based KAIT and Nickel calibrations (hereafter the "Lick calibration") and the UVOT measurements can be achieved. These stars cover a wide range of brightness (from $B = 12.30$ to $B = 19.03$ mag) and color [from $(B - V) = 0.51$ to $(B - V) = 1.39$ mag]. The photometry of SN 2005am itself will provide ground-based estimates for the magnitudes of SN 2005am at the epochs of the UVOT observations, as discussed in §4.

Since the filter transmission curve is a good indication of how standard a filter is, in Figure 3 we show a comparison of the transmission curves for the U, B, and V filters

involved in our analysis, including these used by KAIT (thin solid lines), Nickel (dash-dotted lines), and UVOT (dashed lines). Also plotted are the standard Johnson-Cousins UBV transmission curves (thick solid lines) as described by Bessell (1990). For the B and V filters, the transmission curves generally share the same spectral range and are similar to each other. In particular, the UVOT B and V filters are quite consistent with the Bessell descriptions, so we expect the color terms for these filters to be small, as confirmed later in the paper. For the U filter, however, the one used by KAIT is quite different from the one used by UVOT, and their transmission curves are quite different from the Bessell description. Relatively large color terms for these filters are thus expected, as discussed below.

3. Photometric Calibration of the UVOT

3.1. UVOT Observations of SN 2005am

A journal of UVOT observations of SN 2005am is listed in Table 4. These are the data available to the general users after *Swift* data were made public on 2005 Apr. 1. A more complete set of UVOT data on SN 2005am, some of which were not made available to us, is reported by Brown et al. (2005a). We first retrieved the data from the *Swift* quicklook database, and in all cases, the level-2 filter sky images were downloaded. From the *Swift* manual, the level-2 data are what most researchers will use to start their analysis. The UVOT reduction pipeline has been performed on these images, which are also stored in sky coordinates (RA_{J2000} and DEC_{J2000}). The accompanying exposure maps for each individual image are also downloaded. There are UVOT observations of SN 2005am in other filters ($UVW1$, $UVW2$, and $UVM2$) as well, but these images are not listed in Table 4, and will not be studied in this paper since these filters are in the far-UV where we do not have ground-based calibrations.

There are five UBV sequences observed by UVOT in Table 4, which we hereafter refer to as obs1, obs2, obs3, obs4, and obs5, respectively. The U-band observation in sequence obs1 will be referred as "obs1 U," etc. There is only a short (18.02 s) U-band exposure, and a normal V-band exposure in obs4; the B band is missing. All sequences were observed without binning except obs2, in which a 2×2 on-board binning was used. The SN was well detected in all images except obs4 U and obs5, for which the exposure times were too short for the brightness of the SN. The unbinned UVOT data have a resolution of $0.5''$ per pixel, and the total field of view is $16'.4 \times 16'.4$. Since the fields of view of KAIT ($6'.6 \times 6'.6$) and the Nickel telescope ($6'.3 \times 6'.3$) are much smaller, the field for which we have ground-based calibration is only a fraction of the total UVOT field.

Inspection of the UVOT images reveals two things worth noting for observers familiar with the reduction of ground-based CCD observations. First, as shown in Figure 4 and also indicated in the *Swift* manuals, the PSFs of the stars vary with the count rate (i.e., magnitude) of the object and with the filter being used, and they may vary with position on the detector. The brightest stars also show various degrees of "ghost" emission, including ghost wings, ghost rings, and rings around the stars themselves. This is very different from ground-based CCD images, in which stars of different brightness have a constant PSF across the image (except for image distortion in wide-field images, optical defects, or stars that are saturated). As discussed more in later sections, a varying PSF is a serious challenge for doing stellar photometry, unless the intrinsic PSFs can be constructed according to the brightness of the stars and their positions on the detector. Unfortunately, the information on the intrinsic PSF was not available at the time when we conducted this study.

Another aspect of the UVOT images that is different from ground-based CCD observations is the sky background distribution and the associated noise pattern. Figure 5 shows the histograms of the sky background distribution around star #5 in the first

four U-band observations. The histogram in obs5 U is not shown, but it is similar to that of obs3 U. These background values are extracted from an annular region with an inner radius of 35 pixels and an outer radius of 45 pixels around star #5 for unbinned data, and an inner radius of 17.5 pixels and an outer radius of 22.5 pixels for the 2×2 binned obs2, as discussed more in the next section. As shown in the figure, only in obs2 does the sky background around star #5 show a Gaussian distribution. In the other three observations, due to the low background, the histogram peaks and truncates at background value 0, and shows a Poissonian rather than a Gaussian distribution. This is different from ground-based CCD observations in which the background distribution closely follows photon statistics and is mostly Gaussian. How to optimally account for the background contamination at the location of stars has direct impact on the photometry, as discussed more in the next section.

3.2. Aperture Photometry Parameters

In this paper we use U, B, and V as the magnitudes in the standard Johnson/Cousins *UBVRI* system, such as the calibrated magnitudes for the local standard stars listed in Table 2. We use u, b, and v as the instrumental magnitudes measured from the UVOT image. The "phot" task in the IRAF/DAOPHOT package is used to carry out the aperture photometry throughout the paper. The parameters derived in our paper should be easily adaptable to other photometry programs that work on FITS images.

In theory, if one can properly estimate the sky background and use a very large aperture to sum all the flux, a varying PSF should not be a problem for doing photometry. In practice, however, a big aperture includes more sky background and its associated noise. The signal-to-noise ratio (S/N) for the photometry will thus diminish, so large apertures only work for bright objects. Moreover, because of contamination from neighboring objects, it is often not possible to use large sky regions or apertures when doing photometry.

For the reductions used throughout this paper, we adopt an annular sky background region with an inner radius of 35 pixels and an outer radius of 45 pixels centered on each object for unbinned data, and an inner radius of 17.5 pixels and an outer radius of 22.5 pixels for 2×2 binned data. The full width at half maximum (FWHM) of the UVOT images is about 4.0 pixels (2.5 pixels for the 2×2 binned data), so the sky region starts more than (7–8) $\times$ FWHM from the source, which is further than one generally uses for ground-based photometry [(4–5) $\times$ FWHM]. We thus expect the contamination from the source itself to the background to be small. For bright objects that have ghost emission as shown in Figure 4, there is considerable emission from the source itself in our defined sky region, and we will attempt to evaluate how our analyses can be applied to bright objects in §3.4. Fortunately, for all the local standard stars in the field of SN 2005am, only star #6 is bright and shows a surrounding ring in most of the images. We thus exclude star #6 in our studies in the following sections, but include it in the studies for bright objects in § 3.4.

3.2.1. Optimal Aperture Size

What aperture size should one use in the "phot" program, so that the measured instrumental magnitudes are most consistent with the Lick calibration? To answer this question, we perform photometry for the SN 2005am field stars using aperture radii of 1 to 25 pixels. As a starting point, we use the zero points for the UVOT filters from Table 1. For each aperture radius, the difference between the UVOT photometry and the Lick calibration is calculated for each local standard star, the average difference is calculated, and the RMS around this average is determined. Since the average difference can be corrected by changing the zero point, the RMS around the average difference measures the degree to which the UVOT photometry is consistent with the Lick calibration.

The DAOPHOT package offers various sky background fitting algorithms; see Stetson

(1987) for detailed discussions. In this section, we use a simple "mean" method to determine the sky background. §3.2.4 explores the other algorithms, and concludes that for UVOT observations of SN 2005am, "mean" works best for stars that are not close to other contaminating sources.

Figure 6 shows the RMS versus the aperture size (radius) in pixels. The open circles are for obs1, the solid circles for obs2, the stars for obs3, the solid triangles for obs4, and the solid line for obs5. For obs2 (binned 2×2), the apertures shown in Figure 6 (APT′; solid circles) are the actual aperture sizes (APT) scaled to match the unbinned data. We find the best match to be APT′ = APT×2 − 1, rather than APT′ = APT×2 as one would expect. The cause of this difference is unclear, but we note that the FWHM of obs2 (~ 2.5 pixels) is not exactly half of the other unbinned observations (FWHM ~ 4.0 pixels) either.

Figure 6 indicates that for the B and V bands, the smallest RMS (~ 0.07 mag) is achieved with an aperture size of 5 pixels (3 pixels for 2×2 binned data). This result is consistent with the trend found in ground-based CCD images, where the best S/N is often achieved when the photometry aperture is close to the FWHM. For the U band, the RMS shows a rather flat distribution for apertures in the range 5–12 pixels.

An aperture size of 12 pixels is used in the *Swift* manual to determine the zero points. As shown in Figure 6, however, the RMS at 12 pixels is 0.04–0.10 mag larger than at 5 pixels (up to 0.15 mag larger in obs3 V) for the B and V bands, and is about the same for both apertures in the U band.

We thus find that an aperture radius of 5 pixels (3 pixels for 2×2 binned data) gives the most consistent results between the UVOT photometry and the Lick calibration of the SN 2005am field stars. In sky coordinates, this is $2''.5$, and $3''.0$, respectively.

3.2.2. Preliminary Zero Points

Ideally, the optimal aperture size also gives the most consistent zero point (a source yielding 1 count per second) for the observations. The average differences as calculated in the previous section, which represent the amount to which the UVOT zero point in Table 1 needs to be modified when a specific aperture is used, is plotted in Figure 7. The same symbols are used for the different images as in Figure 6.

We note that with the exception of obs3 V (stars in the lower panel) and obs4 U (triangles in the upper panel), the other curves all converge in the aperture size range of 4–8 pixels, then diverge when the aperture is larger or smaller. An aperture size of 5 pixels indeed gives a very consistent zero point for these observations.

Obs4 U is a short exposure (18.02 s), with most of the background having a value of 0; the local standard stars are not well detected. We remove obs4 U from the zero point determination for the U band, and caution that our U-band zero point may not work for short exposures.

It is puzzling that the well-observed obs3 V gives a different zero point than the other observations. We compare this image to obs1 V. Using a large aperture size of 35 pixels, we measure the total flux for several bright (but without ghost emission) stars, and find that the flux ratios between these stars are inconsistent with the ratio of the exposure times listed in Table 4. From the flux ratios of the stars and the exposure time of obs1 V, the matching exposure time for obs3 V is about 68 s, rather different from 82.77 s as listed in Table 4. The *Swift* UVOT team (Brown et al. 2005c) reported that for GRB 050603, one UVOT exposure was affected by an error in the on-board shift-and-add code, which resulted in a large amount of missing data and an effective exposure time that is much less

than indicated in the FITS header. The "UVOT Digest" page[4] further announced that the exposure time keywords are incorrect for a small fraction of the UVOT images, and a list of such images is provided[5]. Obs3 V is one of the images with wrong exposure time keywords. The corrected exposure time is 60.0 s, slightly different from what we derived from comparing the flux ratio between obs1 V and obs3 V ($\sim$ 68 s).

With obs3 V and obs4 U excluded from the analysis, we measure the following first-order zero points for the UVOT UBV filters, when an aperture size of 5 pixels (3 pixels for the 2×2 binned data) is used: $ZP(U) = 18.22 \pm 0.10$ mag, $ZP(B) = 18.88 \pm 0.09$ mag, and $ZP(V) = 17.67 \pm 0.07$ mag. The uncertainty of the zero point is the quadrature sum of the RMS from the multiple observations and the RMS of the differences between the UVOT photometry and Lick calibration shown in Figure 6. These zero points will be refined in § 3.4. We note here that these zero point uncertainties are overestimated, since part of the RMS between the UVOT photometry and Lick calibration is caused by an intrinsic 0.04–0.05 mag scatter in the UVOT photometry (§ 6.2). Moreover, the UVOT photometry has not been corrected for the coincidence-loss correction, which is necessary even for these relatively faint SN 2005am field stars, as we discuss in § 3.4.

We also note that when an aperture size of 12 pixels is used, the zero points for the UVOT UBV filters from our analysis are $ZP(U) = 18.49 \pm 0.14$ mag, $ZP(B) = 19.16 \pm 0.20$ mag, and $ZP(V) = 17.92 \pm 0.18$ mag. These zero points are consistent with those from the *Swift* calibration database as listed in Table 1 to within the quoted errors. Note that the uncertainties of the zero points with an aperture size of 12 pixels is significantly larger (more than double in B and V) than those with an aperture size of 5 pixels. *We strongly recommend the use of 5-pixel apertures for all UVOT UBV photometry.*

[4]http://swift.gsfc.nasa.gov/docs/swift/analysis/uvot_digest.html

[5]http://swift.gsfc.nasa.gov/docs/swift/analysis/unmatched_exposures.txt .

3.2.3. The Necessity of the Coincidence-Loss Correction

In an attempt to further refine the zero points, the residuals of the UVOT photometry when compared to the Lick calibration have been vigorously studied. The UVOT photometry is measured using the optimal aperture size and zero points as discussed above.

In Figure 8, we show the residual of $b(UVOT) - B(Lick)$ versus the $b(UVOT) - v(UVOT)$ color for the local standard stars in obs1 B. There is no apparent correlation between the residuals and the colors, suggesting that the presence of a large color term is unlikely.

In the upper panel of Figure 9, we show these residuals again, but as a function of $b(UVOT)$. A strong correlation can be seen in this plot. To account for this correlation, a correction factor (CF) needs to be multiplied to the magnitudes measured in the "phot" program. The middle panel of Figure 9 shows that when $CF = 1.07$ is applied to correct for the measured UVOT photometry (with a new zero point of 17.77 mag), the RMS of the photometric differences is significantly improved, from RMS = 0.082 mag to RMS = 0.035 mag.

We analyze all the B-band and V-band images (except obs3 V), and a strong dependence of the residuals on the magnitude is apparent for all the images. The correction factors measured from the images are consistent for the same band (to within errors), but are different for the two bands. We did not attempt to measure a correction factor for the U band because we only have a preliminary U-band calibration for a limited number of stars.

We have performed several analyses to investigate the properties and the possible cause(s) of the correction factor. We find that the correction factor is related to the magnitude (or count rate for the UVOT detectors) rather than the total counts of the final detection (which is a function of both count rate and exposure time). The correction factor

is present in the data reduced with different sky regions or aperture sizes, suggesting that it is not caused by sky background evaluation, or by our choice of a relatively small optimal aperture.

We find that the correction factor is a natural consequence of the coincidence-loss (hereafter C-loss) correction; see the detailed discussion in § 3.4. The bottom panel of Figure 9 shows the residuals of the obs1 B photometry after the C-loss correction, and no apparent correction is present. The RMS after the C-loss correction is 0.041 mag, comparable to that achieved using the correction factor (0.035 mag). This indicates that even for relatively faint (mag 16 to 19) stars, it is necessary to consider the C-loss correction. Since the correction factors and their corresponding zero points can be naturally accounted for in the C-loss correction (§ 3.4), we do not report their values separately here.

3.2.4. Optimal Sky Fitting Algorithm

At the low background count rates found in the UVOT, the distribution of the background in a given aperture is Poissonian, rather than Gaussian as in ground-based optical images. Because of this, some of the usual sky-fitting routines in IRAF are inappropriate to use. In this section we explore the various sky background fitting algorithms offered by IRAF/DAOPHOT. As discussed in more detail by Stetson (1987), DAOPHOT offers the following sky-fitting methods: constant, file, mean, median, mode, centroid, gauss, ofilter, crosscor, histplot, and radplot. Among these, "constant" and "file" require background values supplied by the user, and are not adopted in our reductions. "Gauss" fits a Gaussian function to the background histograms. As shown in Figure 5 and as discussed in §3.1, most of the histograms do not show a Gaussian distribution, so this method is not used. "Histplot" and "radplot" require the user to mark the background interactively, on the histogram and radial profile plot of the background, respectively. We

found it difficult to visually estimate a reasonable background from the plots for many of the observations, and did not include the results from these two methods in our analysis.

Among the six sky-fitting algorithms we used (mean, median, mode, centroid, ofilter, and crosscor), "mean" often outputs the largest background value, while "centroid" outputs the smallest. The "centroid" method often estimates a background value of 0 (as does the "mode" method), since that is where the histogram peaks for many observations; thus, it produces the brightest magnitude measurements among all the methods.

Using our defined sky background region and the optimal aperture size, we analyze obs1 V using all six sky-fitting algorithms. We derive the zero points and their uncertainties, and the correction factor for each sky-fitting method, and list the results in Table 6. Without using CF, all the methods yield consistent zero points and similar uncertainties. The magnitudes measured with the "centroid" method are on average 0.04 mag brighter than with the "mean" method, as indicated by the difference in the zero points. When CF is used, different methods require slightly different values of CF (and the associated zero points). The uncertainties of the zero points are very similar, and are also significantly smaller than those without using CF.

The "mean" method offers a slightly smaller uncertainty than the other methods, and also requires the smallest CF; it is thus preferred by us. We note, however, that the results from different sky-fitting methods do not differ significantly in terms of zero-point uncertainties, at least for an uncrowded field such as the SN 2005am field stars. In §4, we attempt to derive the photometry for SN 2005am in the UVOT images. In this case the different sky-fitting methods yield more significant differences, as SN 2005am is contaminated by a bright nearby star and its host galaxy.

3.3. Observations of SN 2005cf and Landolt Standard Stars

It is important to verify that the photometric parameters we derived from the observations of SN 2005am also work for other UVOT observations, and to include more standard stars to improve the calibrations. For this purpose we have included observations of SN 2005cf, for which the UVOT has multiple-epoch observations in the various filters, and for which we have good ground-based follow-up observations and calibrations.

SN 2005cf was discovered by Pugh & Li (2005) during the course of the Lick Observatory Supernova Search (LOSS; Filippenko 2005) on 2005 May 28. It was classified as a SN Ia more than 10 days before maximum light by Modjaz et al. (2005b) from a spectrum taken with the F. L. Whipple Observatory 1.5-m telescope on 2005 May 31. SN 2005cf was chosen as a target for the *Hubble Space Telescope* (*HST*) GO program 10182 (PI: A. V. Filippenko), and was extensively followed by many groups using ground-based telescopes and by *Swift*/UVOT. A paper on the photometry of SN 2005cf will combine the data from *HST*, *Swift*/UVOT, and the ground-based telescopes (Li et al. 2006, in prep.).

Photometric calibrations of the SN 2005cf field were performed under photometric conditions on 4 nights: 2005 June 3 with KAIT, and 2005 June 3, July 8, and July 11 with the Nickel telescope. The same observation and reduction procedures as described for SN 2005am in § 2 were followed to derive the standard *UBVRI* photometry for the local standard stars in the field of SN 2005cf. Table 6 lists the U, B, and V magnitudes of the local standard stars, and Figure 10 shows a finder chart for the SN 2005cf field. On the night of 2005 July 11 a field (the right panel in Figure 10) that does not include SN 2005cf, but is still included in the UVOT field of view for SN 2005cf, has also been calibrated; this is also the only night that the two fields have been calibrated in the U band. An arbitrary 0.03 mag error is assigned for the stars that have been calibrated only once. Some stars in Table 6 are listed as having been calibrated 5 times in the 4 photometric nights since the

SN 2005cf field was observed twice in the B band on the night of 2005 July 8.

There are many observations of SN 2005cf by UVOT, and we chose the images that have the longest exposure times and also have a complete U, B, and V sequence in our analysis. These data are listed in Table 7.

We also searched the *Swift* quicklook database, found observations for the Landolt standard-star fields "SA104" and "SA95," and included these in our analysis (Table 8). Many of the Landolt standard-star observations have multiple exposures in a single sequence (Column 5 of Table 8), providing multiple measurements for the magnitudes of each individual standard star.

For all the images listed in Tables 7 and 8, we identify the local standard stars in the field of SN 2005cf and the Landolt standard stars, and perform photometry using the optimal parameters derived in the previous sections: the sky background is determined using the "mean" method in a region that is 35 to 45 pixels from the center, and an aperture size of 5 pixels is used. For the photometric zero points, we initially used $ZP(U) = 18.22$ mag, $ZP(B) = 18.88$ mag, and $ZP(V) = 17.67$ mag as derived in § 3.2.2, but changed these to the final zero points as derived in § 3.4: $ZP(U) = 18.24$ mag, $ZP(B) = 18.92$ mag, and $ZP(V) = 17.69$ mag. Adopting the final zero points enables us to directly compare the difference between the UVOT and the standard photometry.

Since there are multiple measurements for the photometry of most standard stars, we average and list their magnitudes in Table 10. For the Landolt standard stars, we exclude those that have been calibrated only once, and those that have calibration errors in excess of 0.05 mag in any of the U, B, or V bands. We also include in Table 10 the averaged photometry for the SN 2005am field stars, but did not include the photometry from the sequence obs2 (binned 2×2) or obs3 (exposure time error). Since the preliminary U-band calibration for the SN 2005am field is inferior to that for the SN 2005cf field, we

did not include the U-band reduction for the SN 2005am field. The errors for the average magnitudes as listed in Table 10 are only the RMS of the multiple measurements, and do not include the photometric error of the individual measurements: we find that when the average photometric error of the individual measurements is added in quadrature to the error, the final uncertainties are overestimated, as the reduced χ^2 is less than unity for the C-loss correction fit in the next section. Since most of the magnitudes have many measurements (8–49), the RMS around the average is probably a more accurate estimate of the true photometric uncertainty. Table 10 provides the basis for deriving the C-loss correction and the final zero points in the next section.

3.4. The C-loss Correction and the Final Photometric Zero Points

In the upper panels of Figures 11, 12, and 13, we compare the UVOT to the standard photometry in the U, B, and V bands, respectively, for all the stars listed in Table 10. The dashed lines in these panels represent the relation where the photometry in the two systems is equal. It can be seen that when the stars get progressively brighter, the UVOT photometry becomes more deviant from the standard photometry, and reaches a limit. This is caused by the C-loss. Here we present a brief introduction to the C-loss and how it is modeled in this paper.

The UVOT detector is a photon-counting device. The photon counter integrates for a short time interval (the readout rate; 11 ms for UVOT); if zero photons arrive during this period, the detector records zero counts. If one photon arrives in this time interval, the detector records one count. *If more than one photon arrives in the interval, the detector still records only one count.* Over a large number of integrations, for a source which sometimes provides more than one photon per time interval, the total measured counts will be *less* than the true counts from the source. This is the cause of the C-loss.

The arrival of photons is a Poisson process. For a source having a true count rate of μ, the probability of getting n photons in the time interval is given by

$$P(n) = \frac{\mu^n}{n!} e^{-\mu} \qquad n = 0, 1, 2, 3, \ldots \tag{1}$$

Without C-loss, if we average over many time intervals, the average measured count rate $\langle n \rangle$ would be

$$\langle n \rangle = 0 \cdot P(0) + 1 \cdot P(1) + 2 \cdot P(2) + 3 \cdot P(3) + \ldots = \sum_{n=0}^{\infty} nP(n) = \sum_{n=0}^{\infty} \frac{n\mu^n}{n!} e^{-\mu} = \mu, \tag{2}$$

which is the true count rate.

With C-loss, however, the measured average count rate x is different from Equation 2. In this case, for $n \geq 2$, the detector records a count of only 1 instead of n, so

$$x = 0 \cdot P(0) + 1 \cdot P(1) + 1 \cdot P(2) + 1 \cdot P(3) + \ldots = 0 + \sum_{n=1}^{\infty} P(n). \tag{3}$$

We note that the sum of $P(n)$ from zero to ∞ must be 1 (because those are all the possibilities for n), so then we have

$$x = \sum_{n=1}^{\infty} P(n) = \sum_{n=0}^{\infty} P(n) - P(0) = 1 - e^{-\mu}. \tag{4}$$

This means that for a photon-counting device with C-loss, such as the UVOT detector, a source that has a true count rate of μ yields a measured count rate of $1 - e^{-\mu}$.

To model the C-loss, we introduce two parameters: ZP and m_∞. ZP is the photometric zero point for the UVOT data, such that a source yielding 1 count per second has a magnitude of 0:

$$m_{\mathrm{UVOT}} = -2.5 \log_{10} \left(\frac{\mathrm{counts}}{\mathrm{sec}} \right) + \mathrm{ZP}. \tag{5}$$

Let m_∞ be the Landolt magnitude that gives a true count rate of 1. Since the measured count rate $(1 - e^{-\mu})$ can only reach 1 when μ is infinity (∞), m_∞ is also the UVOT magnitude that would be measured from an infinitely bright star (the saturation magnitude). For a star that has a Landolt magnitude of $m_{\rm Landolt}$ and a UVOT magnitude of $m_{\rm UVOT}$, we thus have

$$\mu = 10^{-0.4(m_{\rm Landolt} - m_\infty)}, \tag{6}$$

$$1 - e^{-\mu} = 10^{-0.4(m_{\rm UVOT} - m_\infty)}. \tag{7}$$

¿From these two equations we can convert the magnitudes between the UVOT and Landolt systems:

$$m_{\rm UVOT} = -2.5 \log_{10}(1 - e^{-\mu}) + m_\infty, \text{ where } \quad \mu = 10^{-0.4(m_{\rm Landolt} - m_\infty)}; \tag{8}$$

and

$$m_{\rm Landolt} = -2.5 \log_{10}(\mu) + m_\infty, \text{ where } \quad \mu = -\ln(1 - 10^{-0.4(m_{\rm UVOT} - m_\infty)}). \tag{9}$$

We use Eqs. 5 and 8 to fit all the data in Table 10. A χ^2-minimizing technique is used, and the UVOT magnitudes that are too close to m_∞ are not included in the fit (the open circles in Figures 11 to 13). The Landolt standard star 95_42, which has a very blue color $(U - V = -1.33$ mag), is not included in the U-band and B-band fits, but is used in the analysis of the color terms in § 3.5. The best fits to the data are plotted as the solid lines in the upper panels of Figures 11 to 13, and the residuals around the best fits are plotted in the lower panels. The fit parameters are also labeled in the upper panels of the figures. For the final photometric zero points, we derive $ZP(U) = 18.24 \pm 0.01$ mag, $ZP(B) = 18.92$

$\pm$ 0.01 mag, and $ZP(V) = 17.69 \pm 0.01$ mag. For m_∞, we derive $m_\infty(U) = 13.43 \pm 0.02$ mag, $m_\infty(B) = 14.16 \pm 0.02$ mag, and $m_\infty(V) = 12.92 \pm 0.02$ mag. The RMS values of the fits are RMS(U) = 0.080 mag, RMS(B) = 0.044 mag, and RMS(V) = 0.045 mag, and the reduced χ^2 values are $\chi^2(U) = 0.74$, $\chi^2(B) = 0.79$, and $\chi^2(V) = 1.64$, respectively. The reduced χ^2 for the V-band fit (1.64) is a slightly bigger than unity, but is dominated by only a few data points. For example, removing the first two points whose UVOT photometry is close to m_∞ reduced the χ^2 to 1.24.

Our fits to the data in Table 10 provide tight constraints to the photometric zero points ($\sigma = 0.01$ mag) and m_∞ ($\sigma = 0.02$ mag). Applying the C-loss correction also demonstrates that we can derive reliable photometry even when the C-loss is significant (as shown by the residuals in the lower panels of Figures 11 to 13, and the RMS of the fits). Note that $m_{\rm UVOT} \leq m_\infty$ is not allowed because it corresponds to a true flux that is infinite. Stars that give UVOT magnitudes too close to m_∞ should be treated with caution as well. The dash-dotted lines in the lower panels of Figures 11 to 13 indicate the Landolt magnitudes that would give a UVOT magnitude 0.1 mag bigger than the corresponding m_∞: $U = 12.4$ mag, $B = 13.2$ mag, and $V = 12.0$ mag. We tentatively consider these as the limiting bright magnitudes to derive reliable photometry from the UVOT data.

We note that the RMS of the C-loss correction fits, ~ 0.04 mag for B and V, and ~ 0.08 mag for U, represent the photometric precision we can achieve for the UVOT images. The lower panels of Figures 11 to 13 show that although the scatter (and the corresponding error bars) around the fits are bigger when the stars become fainter, scatter is present in the magnitudes for relatively bright stars as well. More discussion of the photometric scatter can be found in § 6.2.

3.5. The UVOT Color Terms

So far in this paper we have treated the UVOT U, B, and V filters as if they follow exactly the standard prescription. As shown in Figure 3, however, the transmission curves for the UVOT filters are somewhat different from the Bessell descriptions, so some color terms are expected. These color terms are listed in the latest calibration data release (2005 Aug. 12) as follows:

$$U - V = 0.087 + 0.8926(u - v) + 0.0274(u - v)^2, \tag{10}$$

$$B - V = 0.0148 + 1.0184(b - v), \tag{11}$$

$$B = b + 0.0173 + 0.0187(u-b) + 0.013(u-b)^2 - 0.0108(u-b)^3 - 0.0058(u-b)^4 + 0.0026(u-b)^5, \text{ and} \tag{12}$$

$$V = v + 0.0006 - 0.0113(b - v) + 0.0097(b - v)^2 - 0.0036(b - v)^3. \tag{13}$$

The uncertainties of the coefficients have not been reported. These equations are only valid for the range of colors $-1.468 < (U - B) < 1.804$ mag, $-1.852 < (U - V) < 3.306$ mag, and $-0.384 < (B - V) < 1.642$ mag.

For the color ranges in which these equations are valid, the difference between B and b (Eq. 12), and also between V and v (Eq. 13), is < 0.02 mag, significantly smaller than the photometric precision that we can achieve in our study (~ 0.04 mag). The color term for $(B - V)$ (Eq. 11) is also small. We thus expect the errors introduced into the UVOT photometry by treating the B and V filters as standard to be small. In Figure 14 we show the residuals of $(B - V) - (b - v)$ versus $(b - v)$, where $(B - V)$ are the colors in the standard system, and $(b - v)$ are the UVOT photometric colors after the C-loss correction. Also overplotted in Figure 14 are three fitting functions: the solid line is $(B - V) = (b - v)$, which is used in this paper; the dashed line is $(B - V) = 1.0148(b - v) - 0.014$, which is

adopted from Eq. 11 but shifted up and down to best match the data; and the dot-dashed line is our best fit to the data: $(B-V) = 0.989(b-v) + 0.004$. The RMS values for the three fits are 0.054 mag, 0.055 mag, and 0.054 mag, and the reduced χ^2 values are 0.64, 0.67, and 0.62, respectively. It is clear from both the RMS and the reduced χ^2 that the three fits do not differ significantly from one another. Thus, unless the UVOT photometric precision can be significantly improved, our data suggest that no color-term corrections for the UVOT B and V bands are necessary.

The results for the $(U-V)$ color are shown in Figure 15. Three fitting function are overplotted: the solid line is $(U-V) = (u-v)$, which is so far used in this paper; the dashed line is $(U-V) = 0.057 + 0.8926(u-v) + 0.0274(u-v)^2$, which is adopted from Eq. 10 but shifted up and down to best match the data; and the dash-dotted line is our best fit to the data, $(U-V) = 0.031 + 0.9150(u-v) + 0.028(u-v)^2$. The RMS values for the fits are 0.089 mag, 0.081 mag, and 0.079 mag, and the reduced χ^2 values are 3.39, 1.31, and 1.09, respectively. Although adopting a color term for the $(U-V)$ color (the dashed and dash-dotted lines) decreases the RMS and the χ^2 of the fit, we note that the blue color end is dominated by just one data point from the Landolt standard star 95_42, and more data for stars with colors $-1.5 < (u-v) < 0.4$ mag are needed to better constrain the coefficients. When the data for 95_42 are excluded from the fit, the three fits give RMS/(reduced χ^2) values of 0.079 mag/(1.11), 0.082 mag/(1.31), and 0.080 mag/(1.08), respectively. Both the RMS and the reduced χ^2 are very similar for the three fits.

To summarize for the $(U-V)$ color, no color term correction is necessary when $(u-v) \geq 0.4$ mag. When $(u-v) < 0.4$ mag, we adopt the best-fit color terms (dash-dotted line in Figure 15). The corresponding correction in the U-band photometry is

$$\Delta = 0.031 - 0.085(u-v) + 0.028(u-v)^2. \quad (14)$$

3.6. Photometry Recipe for the UVOT UBV Filters

In this section we summarize the key parameters and steps involved in performing photometry on UVOT UBV filters. We list all the important parameters required to do photometry in the IRAF/DAOPHOT package (specifically for the program "phot"), but these should be easily exported to other photometry programs.

1. Input all necessary keywords to the datapars of "phot," such as "EXPOSURE" as the FITS keyword for the exposure time.

2. The sky region is defined as an annulus with an inner radius of 35 pixels (17″.5) and an outer radius of 45 pixels (22″.5). That is, in "fitskypars," annulus = 35, and dannulus = 10. For 2×2 binned data, the inner radius becomes 17.5 pixels (17″.5) and the outer radius 22.5 pixels (22″.5). The preferred sky-fitting algorithm is "mean."

3. The photometry aperture is 5 pixels (2″.5) for unbinned data, and 3 pixels (3″.0) for 2×2 binned data.

4. The photometric zero points are $ZP(U) = 18.24$, $ZP(B) = 18.92$, and $ZP(V) = 17.69$ mag. The uncertainties for these zero points are 0.01 mag. The photometry measured from this step are denoted by u, b, and v:

5. Apply the C-loss correction. The UVOT magnitudes after the correction is denoted as u_c, b_c, and v_c.

   $u_c = -2.5 \log_{10} \mu_u + 13.43$, where $\mu_u = -\ln(1 - 10^{-0.4(u-13.43)})$,

   $b_c = -2.5 \log_{10} \mu_b + 14.16$, where $\mu_b = -\ln(1 - 10^{-0.4(b-14.16)})$,

   $v_c = -2.5 \log_{10} \mu_v + 12.92$, where $\mu_v = -\ln(1 - 10^{-0.4(v-12.92)})$.

6. Apply the color-term correction, and derive the standard Johnson/Cousins UBV magnitudes:

$$U = \begin{cases} u_c & \text{if } (u_c - v_c) \geq 0.4 \text{ mag} \\ u_c + \Delta & \text{if } (u_c - v_c) < 0.4 \text{ mag,} \end{cases}$$

where $\Delta = 0.031 - 0.085(u_c - v_c) + 0.028(u_c - v_c)^2$,

$B = b_c$,

$V = v_c$.

4. UVOT Photometry of SN 2005am

In § 3, we used the observations of the SN 2005am and SN 2005cf field stars and the Landolt standard stars, and derived optimal parameters and the C-loss corrections to conduct photometry of UVOT images. In theory, we can simply follow the recipe in § 3.6 and do photometry of SN 2005am in the UVOT images. However, the complex background around the SN (as shown in Figure 1) requires special attention when performing photometry.

As discussed in § 2, in ground-based photometry we used the PSF-fitting technique to fit for the background around the SN and its neighboring bright star, and measured their fluxes simultaneously. Since the PSF is constant across the image and there are plenty of bright and isolated stars, a robust PSF can be constructed, and the overall photometry shows a high degree of self-consistency; see, for example, the final light curves shown in Figure 2. In UVOT images, however, since the intrinsic PSF varies, PSF fitting is not possible without a precise description of the intrinsic PSFs. We note that the UVOT observations of the SN 2005am field could be used to study the intrinsic PSFs, but to better constrain the PSF variation dependence on source brightness and position on the chip, many more observations will be needed than those currently available to us. Therefore, we need to resort to aperture photometry to measure the magnitudes of SN 2005am.

Because of the complex background around SN 2005am, it is vital to use a small aperture for photometry, so that the relatively poor sky-background estimate has less impact on the final photometry. Fortunately, our optimal aperture (5 pixels for unbinned data, and 3 pixels for 2×2 binned data) is small, and is used to derived photometry for SN 2005am. We also adopt all the other photometric parameters derived from the previous section.

In § 3.2.4 we studied several sky-fitting algorithms, and preferred "mean" for uncrowded SN 2005am field stars. However, since our defined sky background region for SN 2005am is affected by its host-galaxy emission, "mean" will almost certainly overestimate the background contribution inside the aperture radius. We thus performed photometry on SN 2005am using several sky-fitting algorithms (mean, mode, centroid, median, ofilter, and crosscor), averaging the final results and also calculating their RMS.

The final photometry of SN 2005am after the C-loss and color-term corrections is listed in Column 3 in Table 11. Because we did not include obs4 U (due to its short exposure) and obs3 V (due to its erroneous exposure time) in the zero-point determination, we did not perform direct photometry of these images. The uncertainties of the photometry are the quadrature sums of the zero-point error, the photometric error from "phot," and the RMS of different sky-fitting methods.

Since we have good B and V, and preliminary U, calibrations for part of the SN 2005am UVOT field from the ground, we can also choose to do differential photometry between the SN and the local standard stars, as listed in Column 4 of Table 11. The UVOT photometric measurements for SN 2005am and the local standard stars are corrected for the C-loss and color-term corrections before performing the differential photometry. The photometric uncertainties are the quadrature sums of the "phot" error, the RMS of the different sky-fitting methods, and the RMS of the photometry when compared to all the

local standard stars. The zero point and its uncertainty are irrelevant in doing differential photometry. For obs4 U and obs3 V, differential photometry is the only way to measure the magnitudes for SN 2005am.

Comparison of the photometry for SN 2005am between the two methods reveals no significant difference. We adopt the differential photometry as it provides measurements for all the images. In Column 5 of Table 8, we list the ground-based estimates for the magnitudes of SN 2005am at the time of the UVOT observations by fitting a smooth spline3 (order 2) curve to the the KAIT/Nickel data after JD 2453450, while Column 6 lists the difference between our adopted UVOT photometry of SN 2005am (Column 4) and the ground-based estimate. We also combine the UVOT photometry of SN 2005am with the ground-based Lick light curves in Figure 16, and redo the MLCS2k2 analysis. Overall, the UVOT photometry agrees well with the ground-based estimates, especially for the observations taken in the first 4 sequences. However, the difference in the obs5 B observation, -0.43 ± 0.15 mag, is quite large. The SN was not well detected in this particular image, and the magnitude may be more seriously affected by the neighboring bright object than in other frames as a result of the short exposure time and poor detection. The parameters in the MLCS2k2 fit for the combined data set do not show any significant changes.

5. UVOT Photometry of GRB 050603

Since *Swift* is designed to study GRBs and related phenomena, in this section we analyzed the UVOT observations of GRB 050603 as a test case for our photometric calibration results. GRB 050603 was recorded by *Swift*/BAT at 6:29:05 on 2005 June 3, and was initially reported as a short GRB (Retter et al. 2005), but was revised to be a long GRB lasting about 10 s (Gotz & Mereghetti 2005). The optical afterglow (OA) was first

identified by Berger & McWilliam (2005) in images taken with the du Pont 2.5-m telescope at Las Campanas Observatory at 3.4 hours after the burst. The GRB was subsequently detected at radio (Cameron 2005) and submillimeter (Barnard et al. 2005) wavelengths. A tentative redshift of $z = 2.821$ was reported by Berger & Becker (2005).

Swift/UVOT began observations of GRB 050603 at 15:42:59 on 2005 Jun. 3, ~ 9.2 hours after the burst. Brown et al. (2005b) reported a 3.6 mag decline within 2 hours of the UVOT observations, though this was debated by Berger (2005). A revised report for the UVOT observations of GRB 050603 was announced by Brown et al. (2005c).

We retrieved the level-2 UVOT data for GRB 050603 from the *Swift* quicklook archive. The data were observed only in the V band, and only those observations obtained in the first several days after the burst were analyzed. These data are organized in two sequences, sw00131560001uvv (11 individual exposures) and sw00131560002uvv (110 individual exposures). Since the OA is faint, we only studied the images with long exposure times.

We closely follow the UVOT photometry recipe as described in § 3.6, and derive the magnitudes for GRB 050603 as listed in Table 12. To provide a consistency check, we also measured a relatively bright and isolated star "s1" in the GRB 050603 field. A finder chart for the OA and "s1" is provided in Figure 17.

Inspection of the magnitudes of "s1" (Column 4 of Table 12) reveals that, although most of the measurements are stable at mag 16.00±0.04, some are apparently deviant and show a significant flux deficit. This is caused by the erroneous exposure times in the image FITS headers as discussed in § 3.2.2. Following the instructions on the "UVOT Digest" page, we listed the corrected exposure times for these images in Column 5 of Table 12. The magnitudes of the OA (Column 7 of Table 12) are measured using the corrected exposure times for these images.

In images when the OA become faint, We coadd several of them to increase the S/N. The midpoint for the single and coadded exposures is calculated as a flux-weighted mean with a power-law decay index of -1.86, as we derive below.

We show our light curve of GRB 050603 (solid circles) in Figure 18. In comparison, we also overplot the reported magnitudes (open circles) from the *Swift* UVOT Team (Brown et al. 2005c), which used the preliminary in-flight zero-point calibration as listed in Table 1. We fit both datasets with a power-law decay and find the decay index to be -1.86 ± 0.06 for the photometry in Table 12 (solid line in Figure 18), and -2.01 ± 0.22 for the data from Brown et al. (2005c) (dashed line in Figure 18)[6]. The reduced χ^2 for both fits is 2.71 and 2.25, respectively, suggesting that either the reported errors for the magnitudes are underestimated, or the bumps and wiggles around the fits are real. We find that to achieve a reduced χ^2 of unity, an additional error of 0.14 mag is required to be added in quadrature to the photometric error in Table 12. As this is much bigger than the photometric scatter after the C-loss correction in the V band as derived in § 3.4 (0.045 mag), we suggest that the fluctuations around the power-law decay fit are real. Similar phenomena have been observed for other GRBs, such as GRB 021004 (e.g., Lazzati et al. 2002), GRB 030329 (e.g., Matheson et al. 2003), and perhaps GRB 021211 (Li et al. 2003b).

Although the two datasets as plotted in Figure 18 are consistent with each other, and their power-law decay fits have similar indices and reduced χ^2, we note that our photometric errors are much smaller than those reported by Brown et al. (2005c) because of our tight constraints on the photometry zero points and the C-loss correction. The uncertainty of our power-law decay index (0.06) is also significantly smaller than that of the *Swift*/UVOT

[6]Brown et al. (2005c) reported a slightly different power-law decay index (-1.97 ± 0.22) for their dataset. The very small difference is probably caused by the different methods for calculating the midpoints of the exposures.

Team (0.22). Thus, our calibration results provide an improvement to the preliminary in-flight photometric zero points.

6. Discussion

6.1. Caveats of Our Photometric Calibration

Although we have included a limited number of Landolt standard stars in our analysis, the main source of our photometric calibration comes from observations of the local standard stars of two supernovae, SN 2005am and SN 2005cf. Some unique characteristics of our calibration are as follows:

(1) The SN field stars extend the calibration to the fainter end. As can be seen in Figures 12 and 13, the Landolt stars are mostly brighter than mag 16, while the SN field stars extend the calibration to mag 19. As the majority of GRB optical afterglows are expected to be detected much fainter than mag 16, it is critical to study the photometric calibration at the fainter end. Moreover, the fainter end provides the anchor point to determine the zero point in the C-loss correction as in § 3.4.

(2) There are many local standard stars in each SN frame. Consequently, the images can be studied one frame at a time, each of which already provides enough information on photometric consistency between the UVOT photometry and the ground-based calibration. The Landolt stars, on the other hand, have a lower density in the UVOT images, especially since many of them are bright and require C-loss correction. It is thus necessary to combine multiple images to get enough statistics, which could introduce unexpected variables that hide the true correlations.

On the other hand, some limitations of our calibration are as follows:

(1) The SN field stars do not have the photometric precision of the Landolt stars. The uncertainties of the SN field stars are mostly 0.02–0.03 mag, while those for the Landolt stars are smaller than 0.01 mag. In particular, there is only a one-time calibration for the U-band of the SN 2005cf field, and a preliminary U-band calibration for the SN 2005am field that has not been used in the final calibration.

(2) The color range of the dataset is somewhat limited. Except for one Landolt star (95_42) that is quite blue, all the other stars have $(B-V) > 0.4$ mag and $(U-V) > 0.4$ mag. More relatively blue stars should be observed and analyzed to better constrain the color terms of the filters, particularly the U band.

Because of these limitations of our calibration, it is envisioned that the calibration results can be further refined in future studies, although we expect the main improvement to be a better constrained color term for the U band. We note that we have already derived tight constraints on the photometric zero points ($\sigma \approx 0.01$ mag) and m_∞ ($\sigma \approx 0.02$ mag), the saturation magnitude used in the C-loss correction.

We also note that we used aperture photometry to analyze all the images, and it is conceivable that when software packages have been developed to do intrinsic PSF fitting in the UVOT images, the photometric zero points would change, and better precision could be achieved.

Our study has not explored all of the possible parameters for UVOT observations, such as different binning choices, extremely short and long exposures, etc. Moreover, we have not correlated the residuals with all possible parameters of UVOT and the detectors.

We emphasize that our photometric zero points and optimal photometric parameters may not work well on short (< 20 s) UVOT exposures, as suggested by obs4 U. Since it is not always possible to take relatively long exposures with UVOT, it is important to

analyze more UVOT images with short exposures to establish their photometric calibrations and optimal photometric parameters. Unfortunately, it is expected that the photometric calibration for the short exposures suffers from larger uncertainties than those derived in this study, as a shorter exposure time generally means lower S/N. Observing brighter stars in the short exposures to increase the S/N is not an option due to the effect of coincidence loss.

We also note that we did not include obs3 V in our photometric zero-point determinations due to the erroneous exposure time in this image. *Since a small fraction of UVOT images are affected by the exposure time anomaly, and not all of them are recognized and documented, users are urged to seek consistency checks when performing photometry on the UVOT images.* For example, differential photometry should be performed whenever possible, either instead of the absolute photometry or as a consistency check. When multiple observations of the same field are available, photometric consistency should be checked with some bright field stars, as we did with "s1" in § 5 for GRB 050603.

6.2. Investigating the Scatter in the UVOT Photometry

It is a bit disappointing that the photometric precision can only be achieved to the 0.04 mag level in our study of UVOT data (§ 3.4). In comparison, ground-based CCD observations with a moderate-sized telescope can easily reach a precision of 0.02 mag or better for Landolt standard stars. The scatter in the UVOT photometry is unlikely to be caused by the photometric zero-point errors, as an error in the zero point will cause a constant offset, not scatter. The lower panels of Figures 11 to 13 suggest that the dispersion in the photometry is present at all source brightnesses; thus, the scatter is probably not all due to photon statistics; rather, part may be intrinsic to the aperture photometry of the UVOT observations.

We note that all raw UVOT images contain systematic modulo-8 fixed-pattern noise ("mod-8 noise" hereafter) as a result of pixel subsampling on the detector. The CCD detector of UVOT has a physical dimension of 385×288 pixels, 256×256 of which are usable for science observations. The detector attains a large format through a centroiding algorithm to the incoming photons by subsampling each physical pixel into 8×8 virtual pixels, thus providing an image of 2048×2048 virtual pixels. This subsampling process introduces faint residuals with a fixed pattern (the mod-8 noise) in the raw UVOT images, which are removed by ground processing (rather than by in-orbit *Swift* processing). The level-2 images we analyzed in our study have been processed by the *Swift* UVOT pipeline, with the mod-8 noise removed. However, as suggested by the *Swift* manual, photometric accuracy is destroyed after removing the fixed-pattern noise, and flux is conserved only within each 8×8 pixel block. Moreover, the fixed-pattern noise is modified around bright sources, and cannot be recovered without a well-calibrated Monte Carlo analysis.

It is possible that the dispersion in our aperture photometry is caused by the reduced photometric accuracy after removing the mod-8 noise. Unfortunately, it is impractical to bin the level-2 images by 8×8 so that the photometric accuracy can be recovered. The pixel scale would be about $4''$ after binning, and the photometry would be severely affected by undersampling the PSF of the stars.

To further investigate the effect of the mod-8 noise and its removal in the UVOT photometry, we downloaded the raw images of obs1 V and experimented with them using the latest HEAsoft 6.0 software supplied by HEASARC. We kept the images in the detector pixel frame, to avoid possible effects introduced by converting them to the sky coordinate image using "uvotxform."[7] "Uvotbadpix" was performed to remove bad pixels,

[7]We have performed the same tests on the sky-coordinate images and the results do not change significantly, suggesting that "uvotxform" is not the cause of the photometric scatter.

"uvotmodmap" was used to remove the mod-8 noises, and "uvotflatfield" was used to remove pixel-to-pixel variations in the image due to detector sensitivity. We also skipped the "uvotmodmap" step and generated an image with the mod-8 noise still included. A difference image was then generated by subtracting the final image with the mod-8 noise removed from the one that skipped "uvotmodmap," and it represents the total effect on the UVOT images before and after the mod-8 noise is removed by the *Swift* pipeline. In effect, the difference image is the mod-8 noise image normalized by the flat field used in "uvotflatfield."

We studied the normalized mod-8 noise image that was applied to obs1 V during our reductions using HEAsoft 6.0. Visual inspection indicates that the image is very flat. When viewed with a large contrast, a faint, large-scale pattern is revealed. When viewed with a small contrast, residuals that correspond to the stars detected in the obs1 V images are apparent. We randomly selected 10,000 positions in this image, and summed the flux inside a 5-pixel radius region (the optimal photometric aperture derived from our study) at each location. The histogram of the fluxes from these measurements shows a Gaussian distribution, with a dispersion of only 0.325 counts (1σ). We also collected the flux inside a 5-pixel radius region centered on each local standard star in the SN 2005am field. The total flux for the SN 2005am field stars on the normalized mod-8 noise image has a range from -7.74 to $+2.67$ counts. Since the total flux for the SN 2005am field stars using a 5-pixel photometry aperture has a range of 175–4400 counts, the effect of either the random flux fluctuation ($\sigma = 0.325$ counts) or the local flux fluctuation (-7.74 to $+2.67$ counts) on the final photometry is smaller than 0.005 mag, which cannot account for the photometric scatter of 0.04–0.08 mag.

Our analysis also suggests that the mod-8 noise removal procedure as implemented in HEAsoft 6.0 has negligible effect on the final photometry of most stars. Only the faintest

stars that are close to the detection limit will suffer from the flux fluctuation of $\sigma = 0.325$ counts (the flux fluctuations for the SN 2005am field stars are larger, but they are rather bright stars). In fact, when the raw image of obs1 V is studied, it yields nearly the same RMS as the processed image with mod-8 noise removed. The reasons for this are that (1) there are not many bad pixels in the UVOT detector, (2) the flat field in the current CALDB database has a constant 1 at all pixels, and (3) the mod-8 noise removal does not change the photometry significantly.

The flat fields as provided by the latest CALDB release (2005 Aug. 12) have a constant 1 at all pixels, i.e., no flat-fielding is really done to remove the pixel-to-pixel sensitivity variations across the chip. If the pixel sensitivity has a variation of 4–5% across the chip, it will introduce an intrinsic scatter on the order of 0.04–0.05 mag to the measured photometry. We consider the dummy flat fields currently being used in the *Swift* UVOT pipeline as the most likely cause of the photometric scatter, and urge in-orbit flat fields to be obtained by observing relatively bright and blank sky regions, or by construction super-sky flat fields from all available UVOT observations. Our early attempt to construct a super-sky flat field for the V band already shows some large-scale structure and variations, suggesting that proper flat-fielding is crucial in improving the precision of the UVOT photometry.

We experimented with artificially smoothing the images by a small amount. When obs1 V is convolved with an elliptical Gaussian function with $\sigma = 1.0$ and 1.5 pixels, the photometric RMS can be slightly improved by about 0.005 mag. As this is not a dramatic improvement, and smoothing (especially with a high σ) will change the zero points at specific photometric aperture radius, we did not re-analyze all the data after some artificial smoothing.

We tried to correlate the scatter in the photometry with the coordinates of the stars on the images, but found no apparent trend.

It is important to reduce the photometric scatter to improve the photometric accuracy of UVOT images, either through finding the cause of the scatter from observations and subsequent pipeline reductions, or by searching for more sophisticated photometric methods than the aperture photometry method we have employed in our study. When the intrinsic PSF variation has been established from more on-flight observations, for example, the PSF-fitting technique may be applied and may yield better photometric precision.

7. Conclusions

In this paper we present an empirical determination of the optimal photometric parameters to analyze UVOT images using software tools that are familiar to ground-based optical astronomers. We consider the effect of the coincidence-loss correction based on a theoretically motivated model, and provide the photometric zero points and their uncertainties in the UVOT U, B, and V filters. Our calibration results come from the analysis of observations of the local standard stars in the SN 2005am and SN 2005cf fields, and a limited number of Landolt standard stars. The main conclusions from our analysis are as follows:

1. The optimal aperture radius to do UVOT photometry, such that the results are most consistent with the ground-based calibration, is small. A radius of 5 UVOT pixels should be used for unbinned data, and 3 pixels for the 2×2 binned data. This is $2''.5$ and $3''.0$ in sky coordinates, respectively.

2. The coincidence-loss correction is important even at relatively faint levels (mag 16 to 19). Based on a theoretically motivated model, we consider the coincidence-loss correction with two parameters, the photometric zero point (ZP) and the saturation magnitude (m_∞), and derive tight constraints on both parameters. We derive

$ZP(U) = 18.24 \pm 0.01$ mag, $ZP(B) = 18.92 \pm 0.01$ mag, $ZP(V) = 17.69 \pm 0.01$ mag, $m_\infty(U) = 13.43 \pm 0.02$ mag, $m_\infty(B) = 14.16 \pm 0.02$ mag, and $m_\infty(V) = 12.92 \pm 0.02$ mag.

3. With proper coincidence-loss correction, reliable photometry can be achieved for stars as bright as $U = 12.4$ mag, $B = 13.2$ mag, and $V = 12.0$ mag.

4. There is a scatter on the order of 0.04–0.08 mag in the final aperture UVOT photometry that cannot be easily accounted for, but is likely to be due to the variation in the pixel sensitivity for the UVOT detectors.

5. The color terms of the UVOT B and V are small, and need not to be considered unless the UVOT photometric precision is significantly improved. The U band needs to be corrected for color terms when the object has a blue color [$(U - V) < 0.4$ mag].

6. In § 3.6 of this paper, we offer a step-by-step photometry procedure for UVOT images, including all the optimal photometric parameters, the photometric zero points, and the proper coincidence-loss correction.

7. We performed photometry of SN 2005am in the UVOT images, and compared the results with those from ground-based observations. The UVOT photometry is generally consistent with the ground-based observations, but the difference increased to ~ 0.5 mag in one measurement when the SN became faint. Part of the cause for this large difference is the complex background region around SN 2005am.

Based on our study of the photometry of UVOT images, we offer the following suggestions for future *Swift*/UVOT observations and calibrations. We advise that on-board binning be avoided for the UVOT observations. Though we were able to analyze the 2×2 binned data, the binning introduces yet another variable in the uncertainties of the

photometric zero points. Many photometric calibration observations should be performed, not only of bright Landolt stars, but also of stars at the fainter end, perhaps to an even fainter level than we have studied in this paper ($V \approx 18$ mag). These calibrations should also be done with exposure times that span a large range, including very short durations (< 20 s). Observations of standard stars with blue colors should be obtained to better constrain the color terms of the filters. A series of observations of the same object should be obtained by varying the pointing so the object is detected at different positions on the chip, to better constrain the uncertainty caused by the PSF variation across the chip. We urge in-orbit flat fields/sensitivity maps to be constructed and implemented in the data reduction pipeline to increase the photometric accuracy.

The work of A.V.F is supported by National Science Foundation grant AST-0307894, NASA/*Swift* grant NNG05GF35G, and the Miller Institute for Basic Research in Science (U.C. Berkeley; Miller Research Professorship). SJ gratefully acknowledges support from a Miller Research Fellowship. KAIT was made possible by generous donations from Sun Microsystems, Inc., the Hewlett-Packard Company, AutoScope Corporation, Lick Observatory, the National Science Foundation, the University of California, and the Sylvia & Jim Katzman Foundation.

REFERENCES

Barnard, V., et al., 2005, GCN Circ. 3515

Barthelmy, S. D., et al., 2005, astro-ph/0507410

Bertin, E., & Arnouts, S 1996, A&AS, 117, 393

Bessell, M. S. 1990, PASP, 102, 1181

Berger, E. 2005, GCN Circ. 3517

Berger, E., & Becker, G. 2005, GCN Circ. 3520

Berger, E., & McWilliam, A. 2005, GCN Circ. 3511

Brown, P. J., et al., 2005a, astro-ph/0506029

Brown, P. J., et al., 2005b, GCN Circ. 3516

Brown, P. J., et al., 2005c, GCN Circ. 3549

Burrows, D. N., et al., 2005, astro-ph/0508071

Cameron, P. B. 2005, GCN Circ. 3513

Filippenko, A. V. 2003, in *From Twilight to Highlight: The Physics of Supernovae*, ed. W. Hillebrandt and B. Leibundgut (Berlin: Springer-Verlag), 171

Filippenko, A. V. 2005, in *The Fate of the Most Massive Stars*, ed. R. Humphreys and K. Stanek (San Francisco: ASP), 34

Filippenko, A. V., Li, W., Treffers, R. R., & Modjaz, M. 2001, in Small-Telescope Astronomy on Global Scales, ed. W.-P. Chen, C. Lemme, & B. Paczyński (San Francisco: ASP), 121

Filippenko, A. V., et al. 1992, AJ, 104, 1543

Gotz, D., & Mereghetti, S. 2005, GCN Circ. 3510

Jha, S. 2002, PhD thesis, Harvard University

Jha, S., Riess, A. G., & Kirshner, R. P. 2006, submitted

Jha, S., et al., 2005, AJ, in press

Landolt, A. U. 1992, AJ, 104, 340

Lazzati, D., Rossi, E., Covino, S. Ghisellini, G., & Malesani, D. 2002, A&A, 396, L5

Li, W., Filippenko, A. V., Chornock, R., & Jha, S. 2003b, ApJ, 586, L9

Li, W., et al. 2000, in Cosmic Explosions, ed. S. S. Holt & W. W. Zhang (New York: American Institute of Physics), 103

Li, W., et al., 2003a, PASP, 115, 453

Matheson, T., et al., 2005, ApJ, 599, 394

Modjaz, M., Kirshner, R., & Challis, P. 2005a, IAU Circ. 8491

Modjaz, M., Kirshner, R., Challis, P., & Berlind, P. 2005b, IAU Circ. 8534

Martin, R., Yamaoka, H., & Itagaki, K. 2005, IAU Circ. 8490

Mason, K. O., et al., 2001, A&A, 365, L36

Pugh, H., & Li, W. 2005, IAU Circ. 8534

Retter, A., et al. 2005, GCN Circ. 3509

Roming, P. W. A., et al., 2005, astro-ph/0507413

Stetson, P. B. 1987, PASP, 99, 191

This manuscript was prepared with the AAS LaTeX macros v4.0.

Table 1. Zero points (ZP; mag) for various *Swift*/UVOT filters from the *Swift* CALDB

Filter	U	B	V	$UVW1$	$UVW2$	$UVM2$
ZP	18.38	19.16	17.88	17.69	17.77	17.29
Error	0.23	0.12	0.09	0.02	0.02	0.23
Aperture (pixels)	12	12	12	24	24	24

Table 2. Photometry of local standard stars in the field of SN 2005am

ID	U	N_U	B	N_B	V	N_V	R	N_R	I	N_I
1	–	–	17.62(01)	2	16.71(03)	3	16.15(01)	2	15.82(02)	2
2	16.80(05)	1	16.90(01)	2	16.39(02)	3	16.08(02)	2	15.75(02)	2
4	16.78(05)	1	15.59(01)	2	14.55(02)	2	13.73(01)	2	13.24(01)	2
5	17.16(05)	1	17.14(01)	2	16.56(02)	3	16.13(02)	2	15.79(02)	3
6	12.39(05)	1	12.30(02)	4	11.99(01)	3	11.78(03)	3	11.58(02)	2
7	–	–	18.20(01)	2	17.22(03)	4	16.55(03)	3	16.07(03)	2
9	–	–	17.79(02)	3	17.23(03)	2	16.96(03)	3	16.63(01)	3
10	–	–	17.94(01)	4	17.09(02)	2	16.51(01)	2	15.93(01)	2
12	16.15(05)	1	15.57(03)	4	14.76(01)	3	14.30(02)	2	13.88(01)	2
13	–	–	19.03(03)	1	17.63(03)	1	16.67(02)	2	15.79(02)	2
14	–	–	17.38(03)	3	16.53(01)	2	16.12(01)	3	15.75(02)	4
15	–	–	16.73(01)	2	15.95(03)	1	15.56(03)	2	15.13(03)	1
16	–	–	17.73(01)	3	17.13(02)	3	16.71(03)	3	16.40(02)	4
17	–	–	17.43(01)	2	16.77(03)	1	16.39(01)	2	16.03(03)	2
18	–	–	17.62(01)	4	16.91(02)	4	16.50(03)	4	16.16(02)	4
19	–	–	18.35(02)	2	17.40(02)	4	16.83(02)	4	16.37(03)	4
20	–	–	17.31(01)	4	16.55(03)	3	16.12(03)	3	15.71(02)	4
21	16.22(05)	1	15.55(01)	4	14.70(02)	4	14.22(02)	3	13.76(02)	4
22	15.02(05)	1	14.98(01)	4	14.47(03)	3	14.18(03)	4	13.90(02)	4
23	–	–	18.02(01)	2	17.35(02)	4	16.97(02)	4	16.59(01)	4
24	–	–	17.48(01)	2	16.54(02)	4	15.93(01)	4	15.45(02)	4
26	–	–	16.49(02)	4	15.38(02)	4	14.68(01)	4	14.12(01)	4
27	–	–	17.20(03)	1	16.30(02)	2	15.83(01)	2	15.37(01)	2
28	–	–	17.60(02)	2	16.98(01)	2	16.60(04)	2	16.23(04)	2

Table 3. Lick Observatory photometry of SN 2005am

JD − 2450000	U (mag)	B (mag)	V (mag)	R (mag)	I (mag)	Tel.
3435.83	–	–	–	13.73(03)	13.90(03)	KAIT
3436.76	–	13.90(04)	13.80(04)	13.70(04)	13.93(05)	KAIT
3438.74	–	13.92(02)	13.75(03)	13.65(03)	13.96(04)	KAIT
3439.77	–	13.98(02)	13.78(02)	13.66(03)	13.97(03)	KAIT
3440.74	–	14.04(03)	13.79(03)	13.69(03)	14.01(04)	KAIT
3441.75	–	14.10(02)	13.81(03)	13.73(02)	14.03(02)	Nickel
3442.69	–	14.18(03)	13.84(03)	13.82(04)	14.15(05)	KAIT
3443.76	–	14.27(02)	13.89(03)	13.90(02)	14.18(02)	Nickel
3444.73	–	14.37(03)	13.95(03)	13.99(02)	14.26(03)	Nickel
3444.76	–	14.43(03)	13.98(04)	14.03(03)	14.32(05)	KAIT
3445.77	–	14.53(02)	14.05(02)	14.10(05)	14.39(03)	KAIT
3446.75	–	–	14.12(04)	–	–	KAIT
3455.75	–	15.90(04)	14.72(03)	14.39(04)	14.21(03)	KAIT
3460.73	–	16.46(02)	15.17(02)	14.76(03)	14.42(04)	KAIT
3462.73	–	16.59(02)	15.35(02)	14.97(03)	14.61(03)	KAIT
3465.70	–	16.78(02)	15.55(04)	15.21(03)	14.88(05)	KAIT
3466.69	17.02(0.08)	16.86(05)	15.62(04)	15.21(04)	14.96(06)	KAIT
3467.73	–	16.87(03)	15.65(03)	15.30(03)	15.05(04)	KAIT
3470.77	–	16.99(02)	15.77(03)	15.38(05)	15.09(04)	Nickel
3471.68	–	17.01(03)	15.79(04)	15.47(02)	15.15(03)	Nickel
3471.68	–	17.02(03)	15.81(05)	15.49(04)	15.25(05)	KAIT
3472.73	–	17.01(03)	15.91(03)	15.57(04)	15.39(04)	KAIT
3474.71	–	17.10(03)	15.92(04)	15.64(03)	15.44(04)	KAIT
3477.67	–	17.15(05)	16.03(06)	15.75(04)	15.58(06)	KAIT
3486.66	–	17.40(04)	16.31(03)	16.06(03)	16.02(03)	KAIT
3492.67	–	–	–	16.30(03)	–	KAIT

Note: Uncertainties are indicated in parentheses; these are quadrature sums of the PSF-

Table 4. Journal of *Swift*/UVOT observations of SN 2005am in UBV

Data ID	Obs ID	Date	Filter	UT Start	Exp. time(s)
			U	11:38:44	201.76
obs1	sw00030010070	2005-04-04	B	11:42:14	169.41
			V	11:18:09	201.77
			U	08:39:02	209.77
obs2[a]	sw00030010071	2005-04-06	B	08:42:39	144.23
			V	08:28:12	209.77
			U	02:23:41	82.78
obs3	sw00030010072	2005-04-10	B	02:25:10	40.61
			V	02:15:04	82.77
obs4	sw00030010073	2005-04-22	U	02:24:07	18.02
			V	02:08:03	157.78
obs5	sw00030010076	2005-05-17	U	03:22:59	72.78
			B	03:25:04	46.68
			V	03:15:29	72.77

[a]These data are binned 2×2.

Table 5. Comparison of different sky background fitting algorithm for obs1 V

	Without CF		With CF		
Algorithm	ZP	σ(ZP)	CF	ZP	σ(ZP)
mean	17.68	0.067	1.046	16.95	0.043
mode	17.69	0.074	1.060	16.77	0.044
median	17.69	0.072	1.060	16.76	0.043
centroid	17.73	0.094	1.090	16.38	0.049
ofilter	17.69	0.073	1.060	16.76	0.043
crosscor	17.70	0.078	1.070	16.63	0.044

Table 6. Photometry of local standard stars in the field of SN 2005cf

ID	U	N_U	B	N_B	V	N_V
1	–	–	15.27(01)	3	14.38(01)	3
2	13.65(03)	1	13.49(01)	3	12.80(01)	3
3	16.37(03)	1	15.62(01)	4	14.68(01)	3
4	16.58(03)	1	16.47(01)	3	15.76(01)	3
5	15.31(03)	1	15.33(01)	4	14.82(01)	4
6	14.01(03)	1	14.06(02)	5	13.60(01)	4
7	18.30(03)	1	18.43(01)	4	17.79(01)	2
8	18.93(03)	1	17.81(02)	5	16.26(01)	4
9	15.83(03)	1	15.66(02)	5	14.99(01)	4
10	18.29(03)	1	17.12(01)	5	15.95(01)	3
11	14.96(03)	1	14.75(01)	5	14.02(01)	4
12	19.35(03)	1	18.34(01)	4	17.33(01)	4
13	15.34(03)	1	14.76(01)	5	13.88(01)	4
14	18.56(03)	1	18.14(02)	5	17.39(02)	4
15	18.30(03)	1	17.59(01)	5	16.72(01)	4
16	17.93(03)	1	17.98(02)	4	17.45(01)	4
17	19.02(03)	1	18.21(03)	1	17.23(03)	1
18	15.37(03)	1	14.97(03)	1	14.16(03)	1
20	16.43(03)	1	15.95(03)	1	15.13(03)	1
21	–	–	18.50(03)	1	17.01(03)	1
22	17.95(03)	1	17.20(03)	1	16.25(03)	1
23	17.36(03)	1	17.32(03)	1	16.70(03)	1
24	–	–	19.06(03)	1	17.55(03)	1
25	14.47(03)	1	14.41(03)	1	13.78(03)	1
26	16.38(03)	1	16.07(03)	1	15.30(03)	1

Table 7. *Swift*/UVOT observations of SN 2005cf analyzed in this paper

Obs ID	Date	Filter	N(image)[a]	Exp. time(s)[b]
sw00030028007	2005-06-04	U	1	71.77
sw00030028007	2005-06-04	B	1	71.78
sw00030028007	2005-06-04	V	1	71.78
sw00030028010	2005-06-05	U	1	77.78
sw00030028010	2005-06-05	B	1	59.24
sw00030028010	2005-06-05	V	1	77.77
sw00030028013	2005-06-06	U	1	77.78
sw00030028013	2005-06-06	B	1	57.65
sw00030028013	2005-06-06	V	1	77.77
sw00030028022	2005-06-09	U	1	91.78
sw00030028022	2005-06-09	B	1	69.78
sw00030028022	2005-06-09	V	1	91.76
sw00030028025	2005-06-10	U	1	85.75
sw00030028025	2005-06-10	B	1	67.78
sw00030028025	2005-06-10	V	1	85.77
sw00030028058	2005-06-29	U	1	71.78
sw00030028058	2005-06-29	B	1	51.63
sw00030028058	2005-06-29	V	1	71.77
sw00030028064	2005-07-12	U	1	70.78
sw00030028064	2005-07-12	B	1	49.16
sw00030028064	2005-07-12	V	1	70.78
sw00030028066	2005-07-23	U	1	439.78
sw00030028066	2005-07-23	B	1	414.01
sw00030028066	2005-07-23	V	1	439.77

[a]Number of images in the sequence.

[b]Total exposure time in the whole sequence.

Table 8. *Swift*/UVOT observations of the Landolt fields analyzed in this paper

Obs ID	Object	Date	Filter	N(image)[a]	Exp. time(s)[b]
sw00055450008	SA104NE	2005-04-05	V	1	737.52
sw00055400016	SA104N	2005-04-19	V	1	1146.12
sw00055450010	SA104NE	2005-04-19	V	1	697.78
sw00055350013	SA104SW	2005-05-10	V	1	180.04
sw00054350014	SA95SW	2005-07-07	U	5	1435.88
sw00054350014	SA95SW	2005-07-07	B	5	1295.40
sw00054350014	SA95SW	2005-07-07	V	5	1435.81
sw00054350015	SA95SW	2005-07-08	U	13	6474.45
sw00054350015	SA95SW	2005-07-08	B	13	6080.93
sw00054350015	SA95SW	2005-07-08	V	13	6473.04
sw00054350016	SA95SW	2005-07-11	U	29	11260.67
sw00054350016	SA95SW	2005-07-11	B	29	10009.79
sw00054350016	SA95SW	2005-07-11	V	29	11276.28
sw00054350017	SA95SW	2005-07-09	U	3	1601.43
sw00054350017	SA95SW	2005-07-09	B	3	1511.64
sw00054350017	SA95SW	2005-07-09	V	3	1601.35
sw00055763001	SA95-42	2005-07-07	B	1	568.48
sw00055763002	SA95-42	2005-07-07	V	1	509.65
sw00055763003	SA95-42	2005-07-07	B	1	569.41
sw00055763004	SA95-42	2005-07-07	V	1	509.00

[a]Number of images in the sequence.

[b]Total exposure time in the whole sequence.

Table 9. The average *Swift*/UVOT photometry for the standard stars[a,b]

Name	U	B	V	u	N(u)	b	N(b)	v
95_101	13.718(011)	13.455(004)	12.677(003)	14.127(017)	49	14.347(023)	49	13.296(014)
95_15	12.171(004)	12.014(001)	11.302(001)	13.472(011)	2	14.123(029)	2	12.874(007)
95_16	16.941(037)	15.619(020)	14.313(012)	16.943(065)	2	15.805(014)	2	14.528(016)
95_42	14.280(011)	15.391(009)	15.606(006)	14.353(013)	34	15.648(026)	34	15.703(025)
95_43	11.297(004)	11.313(003)	10.803(002)	13.467(061)	29	14.275(171)	29	12.881(033)
95_96	10.229(004)	10.157(002)	10.010(002)	13.863(665)	21	15.115(1265)	21	13.166(494)
95_97	16.104(031)	15.724(023)	14.818(001)	16.173(035)	48	15.889(039)	48	14.946(024)
95_98	16.721(018)	15.629(002)	14.448(001)	16.779(033)	49	15.794(032)	49	14.621(021)
104_335	12.432(010)	12.287(010)	11.665(010)	–	–	–	–	12.948(030)
104_367	16.357(037)	16.483(033)	15.844(025)	–	–	–	–	15.900(052)
104_484	16.162(024)	15.430(020)	14.406(007)	–	–	–	–	14.640(018)
104_485	16.348(042)	15.855(036)	15.017(011)	–	–	–	–	15.141(032)
sn05cf_1	–	15.265(010)	14.380(007)	–	–	15.470(028)	8	14.558(030)
sn05cf_2	13.650(030)	13.486(012)	12.799(013)	14.078(015)	8	14.332(008)	8	13.341(011)
sn05cf_3	16.370(030)	15.625(008)	14.676(012)	16.428(031)	8	15.751(047)	8	14.766(033)
sn05cf_4	16.582(030)	16.466(008)	15.756(007)	16.577(062)	8	16.501(038)	8	15.805(043)
sn05cf_5	15.311(030)	15.328(011)	14.820(011)	15.437(035)	8	15.491(023)	8	14.901(030)
sn05cf_6	14.014(030)	14.059(027)	13.604(014)	14.338(013)	8	14.585(016)	8	13.866(021)
sn05cf_7	18.297(030)	18.434(017)	17.786(001)	18.215(078)	8	18.406(099)	8	17.783(166)
sn05cf_8	18.926(030)	17.810(020)	16.264(007)	18.925(187)	8	17.788(100)	8	16.213(055)
sn05cf_9	15.831(030)	15.660(023)	14.986(010)	15.858(022)	8	15.799(037)	8	15.035(043)
sn05cf_10	18.294(030)	17.124(016)	15.947(011)	18.277(108)	8	17.142(057)	8	15.951(073)
sn05cf_11	14.956(030)	14.747(008)	14.022(005)	15.081(031)	8	15.044(022)	8	14.219(032)
sn05cf_12	19.353(030)	18.338(012)	17.327(017)	19.305(227)	8	18.342(143)	8	17.300(094)
sn05cf_13	15.340(030)	14.760(006)	13.883(006)	15.424(030)	8	15.056(020)	8	14.088(021)
sn05cf_14	18.558(030)	18.139(025)	17.393(027)	18.298(142)	8	18.093(093)	8	17.375(086)
sn05cf_15	18.297(030)	17.591(011)	16.715(007)	18.172(069)	8	17.611(067)	8	16.708(055)
sn05cf_16	17.933(030)	17.981(020)	17.450(015)	17.902(095)	8	17.992(090)	8	17.409(182)
sn05cf_17	19.016(030)	18.214(030)	17.233(030)	19.079(124)	8	18.330(133)	8	17.301(100)
sn05cf_18	15.370(030)	14.970(030)	14.161(030)	15.479(034)	8	15.203(032)	8	14.362(032)
sn05cf_20	16.435(030)	15.948(030)	15.133(030)	16.443(045)	8	16.024(038)	8	15.224(057)
sn05cf_21	–	18.497(030)	17.008(030)	–	–	18.447(186)	8	16.976(091)
sn05cf_22	17.954(030)	17.200(030)	16.255(030)	17.840(081)	8	17.204(084)	8	16.252(077)
sn05cf_23	17.361(030)	17.322(030)	16.703(030)	17.384(082)	8	17.289(067)	8	16.718(068)
sn05cf_24	–	19.058(030)	17.549(030)	–	–	19.117(253)	8	17.644(074)
sn05cf_25	14.470(030)	14.414(030)	13.780(030)	14.659(023)	8	14.797(010)	8	14.010(015)
sn05cf_26	16.381(030)	16.073(030)	15.297(030)	16.346(055)	8	16.152(016)	8	15.346(035)
sn05cf_27	15.401(030)	14.565(030)	13.546(030)	15.535(039)	8	14.911(019)	8	13.846(009)
sn05cf_28	17.487(030)	17.456(030)	16.853(030)	17.437(051)	8	17.471(043)	8	16.847(085)
sn05cf_29	18.587(030)	18.286(030)	17.516(030)	18.824(150)	8	18.393(152)	8	17.493(122)
sn05cf_30	18.757(030)	18.488(030)	17.754(030)	18.773(180)	8	18.466(223)	8	17.733(208)
sn05cf_31	18.601(030)	18.225(030)	17.504(030)	18.535(106)	8	18.260(101)	8	17.426(127)
sn05cf_32	16.265(030)	15.879(030)	15.016(030)	16.407(053)	8	15.971(024)	8	15.095(045)
sn05cf_33	15.822(030)	15.462(030)	14.682(030)	15.857(030)	8	15.612(034)	8	14.779(029)

Table 10. Aperture photometry parameters for *Swift*/UVOT[a]

Parameter	Value
Sky region	35−45 pixels (17.5−22.5 for 2×2 binned data)
Sky fitting algorithm	mean (but see text for crowded regions)
Aperture size	5 pixels (3 pixels for 2×2 binned data)
ZP(U)	18.24±0.01
ZP(B)	18.92±0.01
ZP(V)	17.69±0.01
$m_\infty(U)$	13.43±0.02
$m_\infty(B)$	14.16±0.02
$m_\infty(V)$	12.92±0.02

[a]See § 3.4 for a complete recipe on how to use these parameters to do photometry on UVOT images.

Table 11. *Swift*/UVOT photometry of SN 2005am

JD − 2450000	Filter	Mag1[a] (mag)	Mag2[b] (mag)	Mag(Lick)[c] (mag)	Diff.[d] (mag)
3464.986	U	17.11(06)	17.13(08)	–	–
3464.989	B	16.85(05)	16.86(06)	16.73(03)	0.13(07)
3464.973	V	15.49(04)	15.52(05)	15.50(02)	0.02(06)
3466.862	U	17.11(09)	17.14(11)	17.02(08)	0.12(12)
3466.864	B	16.85(06)	16.88(09)	16.86(05)	0.02(10)
3466.855	V	15.52(04)	15.53(05)	15.62(04)	−0.09(06)
3470.600	U	17.23(09)	17.28(12)	–	–
3470.601	B	16.97(08)	16.99(10)	16.99(02)	−0.00(11)
3470.594	V	–	15.76(12)	15.77(03)	−0.01(13)
3482.600	U	–	17.54(15)	–	–
3482.590	V	16.20(06)	16.19(09)	16.18(04)	0.01(09)
3507.641	U	18.17(14)	18.23(15)	–	–
3507.642	B	17.49(08)	17.51(14)	17.94(08)	−0.43(15)
3507.636	V	16.84(11)	16.86(14)	17.02(06)	−0.16(15)

[a]Magnitude measured following the UVOT photometry recipe as described in § 3.4.

[b]Magnitude measured from differential photometry.

[c]Magnitude measured (or extrapolated) from Lick Observatory observations.

[d]The difference between Column 4 and Column 5.

Table 12. *Swift*/UVOT photometry of GRB 050603

Date	UT	EXP(s)[a]	Mag(S1)[b]	EXP(s)/[c]	t(mid)(h)[d]	Mag(OA)	σ(Mag)
Jun-03	15:42:59	209.77	15.98	...	9.26	18.30	0.13
Jun-03	15:46:32	1297.63	15.97	...	9.47	18.19	0.06
Jun-03	17:19:24	209.78	15.98	...	10.87	18.49	0.14
Jun-03	17:22:57	1500.44	18.89[e]	109.83	10.91	18.41	0.17
Jun-03	18:55:52	209.76	15.99	...	12.48	18.74	0.16
Jun-03	18:59:21	1772.35	16.00	...	12.75	19.19	0.08
Jun-03	20:32:17	209.77	15.98	...	14.08	19.01	0.19
Jun-03	20:35:50	2103.78	15.99	...	14.40	19.30	0.09
Jun-03	22:12:17	1199.90	15.99	...	15.89	19.37	0.12
Jun-04	00:04:22	1204.78	15.99	...	17.76	19.47	0.12
Jun-04	01:25:45	2055.79	16.00	...	19.23	20.07	0.14
Jun-04	03:03:35	1947.77	15.99	...	20.85	20.13	0.15
Jun-04	04:38:45	2055.78	16.06	...	22.45	20.48	0.19
Jun-04	11:05:35	1947.78	15.99	...			
Jun-04	12:39:44	848.78	15.97	...			
Jun-04	14:16:44	848.78	16.00	...			
Combined		3645.34	...	...	29.84	20.48	0.14
Jun-04	15:53:04	1047.79	16.00	...			
Jun-04	17:29:28	1304.79	16.04	...			
Jun-04	19:05:33	1355.78	16.04	...			
Jun-04	20:44:10	1697.79	17.99[e]	277.25			
Jun-04	22:19:10	1097.78	15.98	...			
Jun-04	23:56:40	1998.78	17.22[e]	614.02			
Jun-05	01:32:38	2004.78	15.99	...			
Combined		10507.49	...	7702.17	38.22	20.91	0.11
Jun-05	09:35:40	1997.79	15.99	...			
Jun-05	11:10:40	1398.78	15.98	...			
Jun-05	12:46:30	697.78	16.01	...			
Jun-05	14:22:44	848.77	15.97	...			
Jun-05	16:00:05	1047.77	16.01	...			
Jun-05	17:35:20	1255.68	16.09	...			
Jun-05	19:12:53	1555.77	19.02[e]	119.02			
Combined		8802.34	...	7365.59	54.63	21.75	0.23
Jun-05	20:50:15	1747.78	16.00	...			
Jun-05	22:27:34	1948.78	15.99	...			
Jun-06	00:03:40	1998.78	16.35[e]	1319.79			
Jun-06	01:38:43	2055.77	15.98	...			
Jun-06	03:15:18	2025.79	16.05	...			
Combined		9776.90	...	9097.91	65.82	>22.21	0.32

[a]Original exposure time (in seconds) in the FITS file.

[b]Magnitude of S1. Most of the measurements are stable at mag 16.00±0.04, but some are apparently deviant.

Fig. 1.— Finder charts for the field of SN 2005am. The left panel shows a KAIT R-band image ($6'.6 \times 6'.6$) taken on 2005 Mar. 13, and the right panel shows a Nickel R-band image ($6'.3 \times 6'.3$) taken on 2005 Mar. 12. North is up and east is to the left. SN 2005am and the local standard stars listed in Table 2 are labeled.

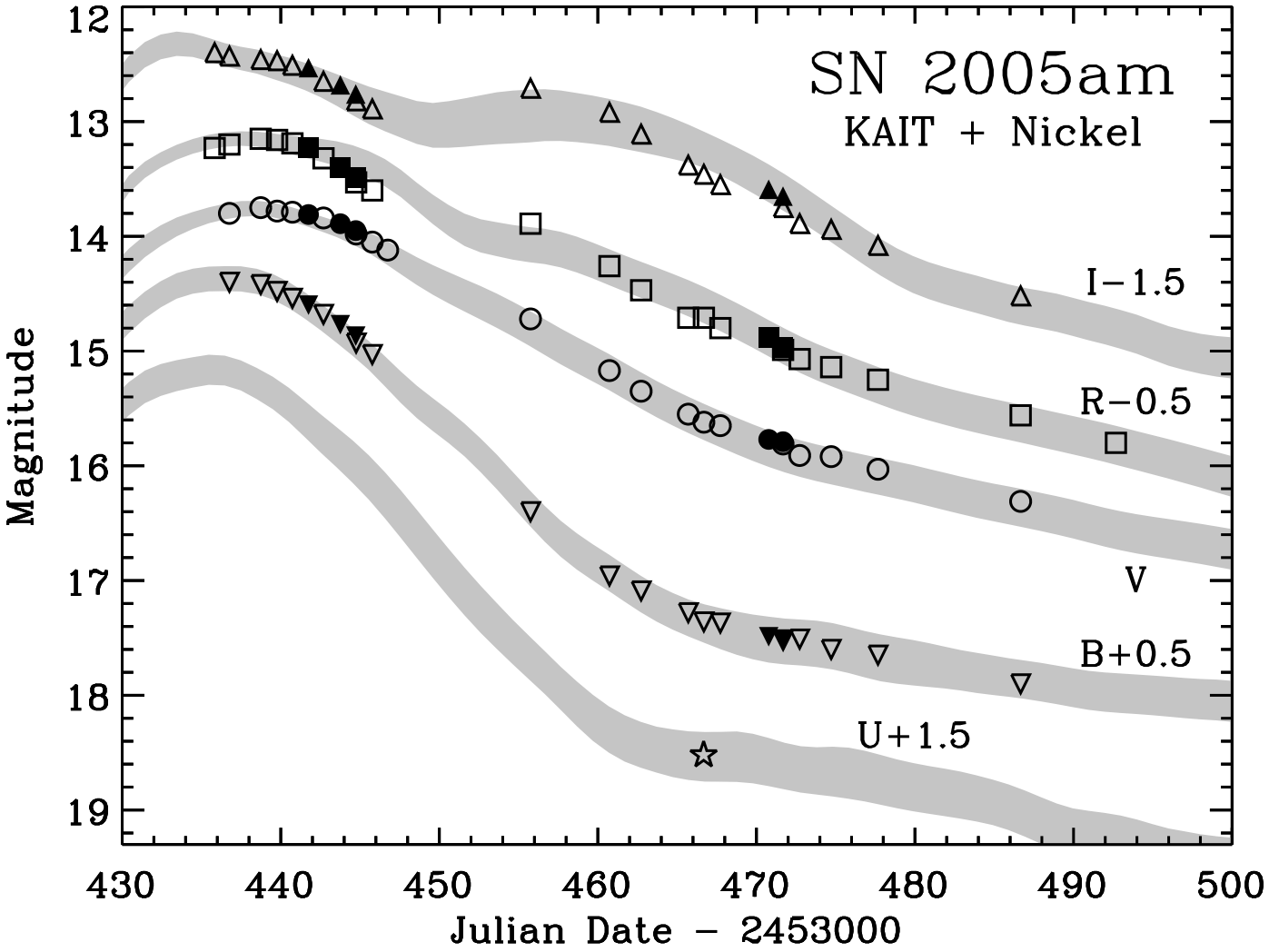

Fig. 2.— The ground-based photometry of SN 2005am. The solid symbols are from the Nickel telescope, and the open symbols are from KAIT. Also overplotted are the MLCS fits.

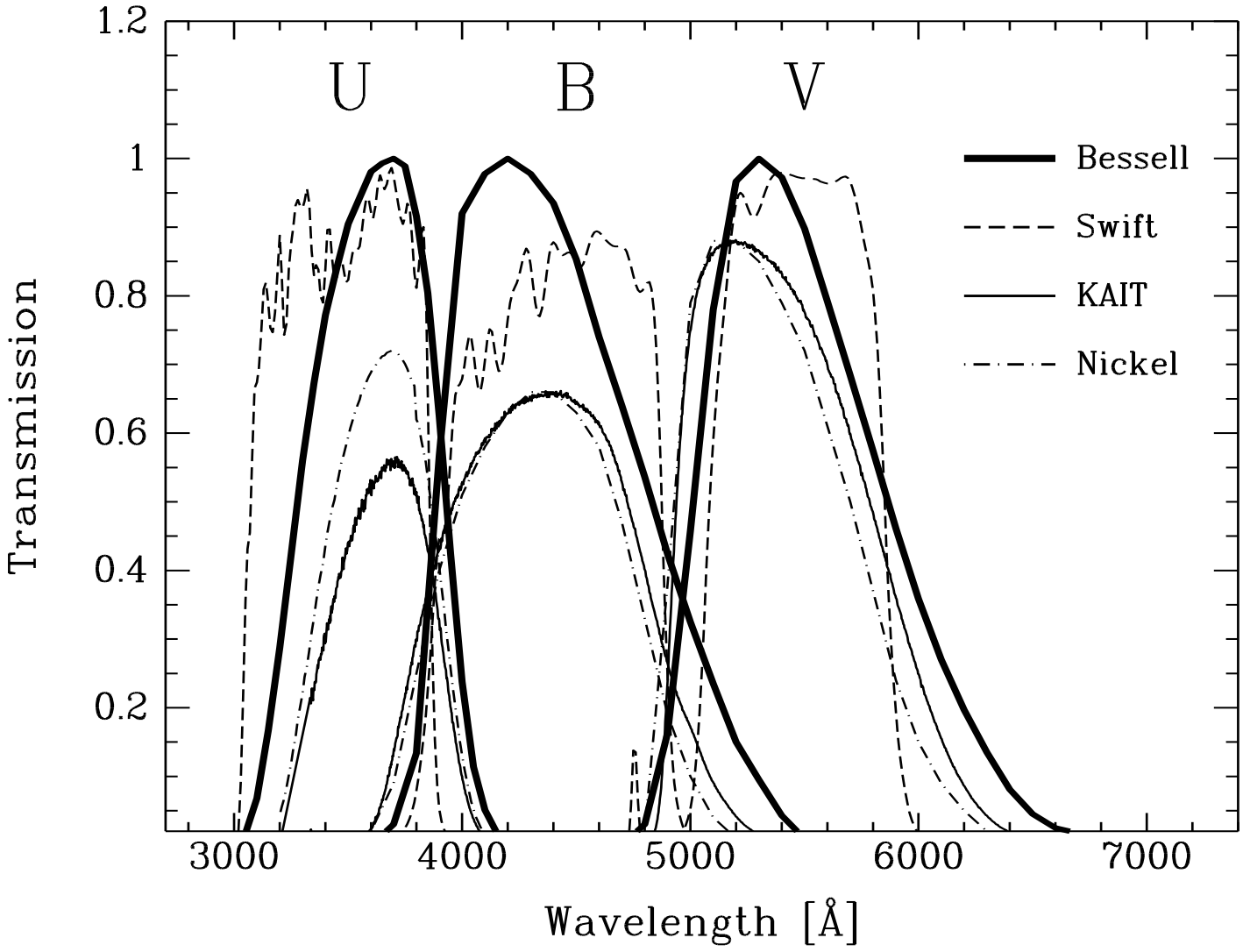

Fig. 3.— The U, B, and V filter transmission curves. Plotted are the filters used by KAIT (thin solid lines), Nickel (dash-dotted lines), and UVOT (dashed lines). The Bessell (1990) descriptions are plotted as thick solid lines.

Fig. 4.— Sample PSFs of stars in the UVOT obs1 V image. (1) A very bright star with ghost wings (a), ghost ring (b), and ring (c); (2) a pair of bright stars with ghost rings (b) and rings (c); (3) a bright star with ring (c); and (4) stars with no ghost emission, but with varying profiles.

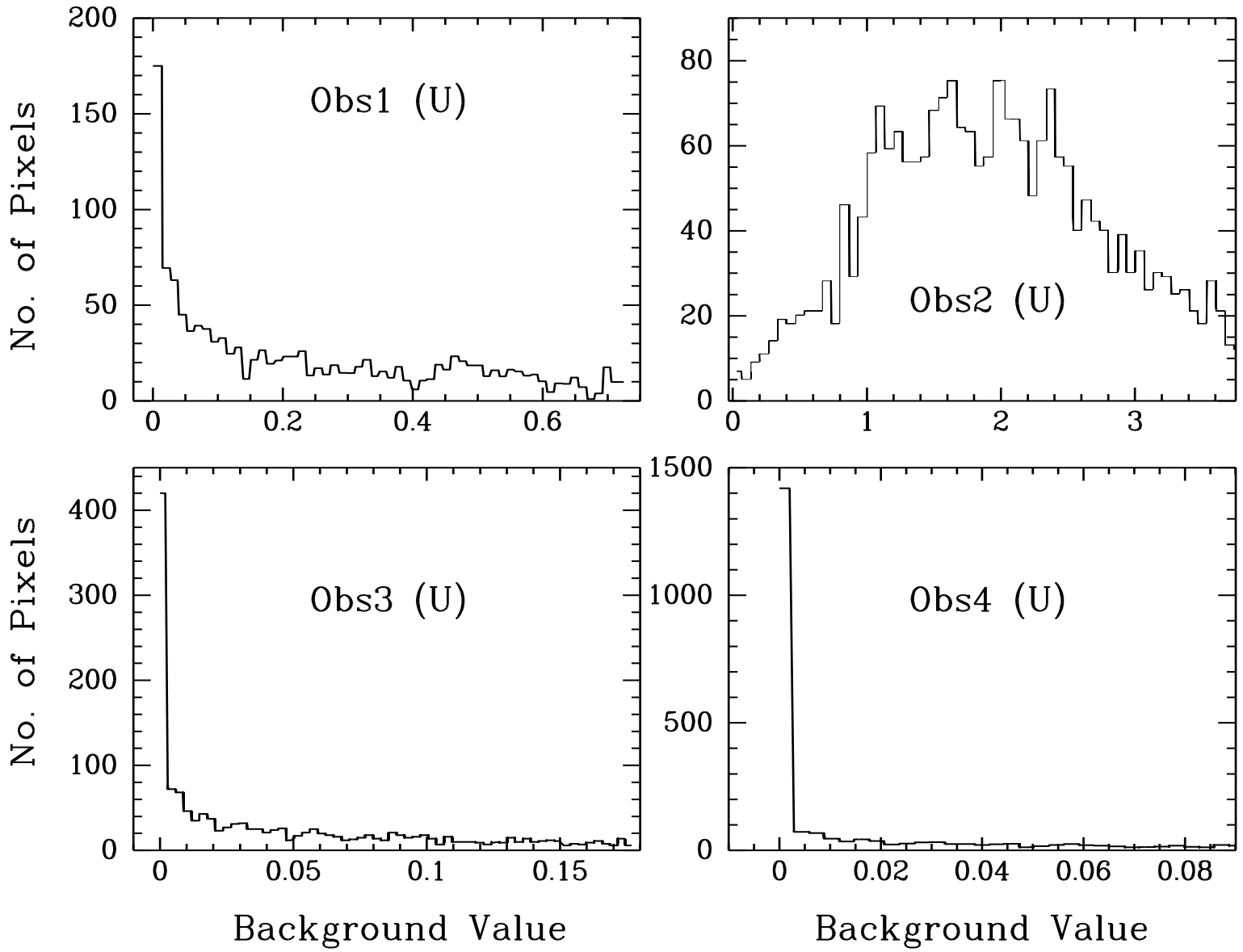

Fig. 5.— The histogram of sky background around star #5 in the four U-band observations. Only obs2 has a Gaussian-like distribution. The other distributions peak and truncate at a zero sky value.

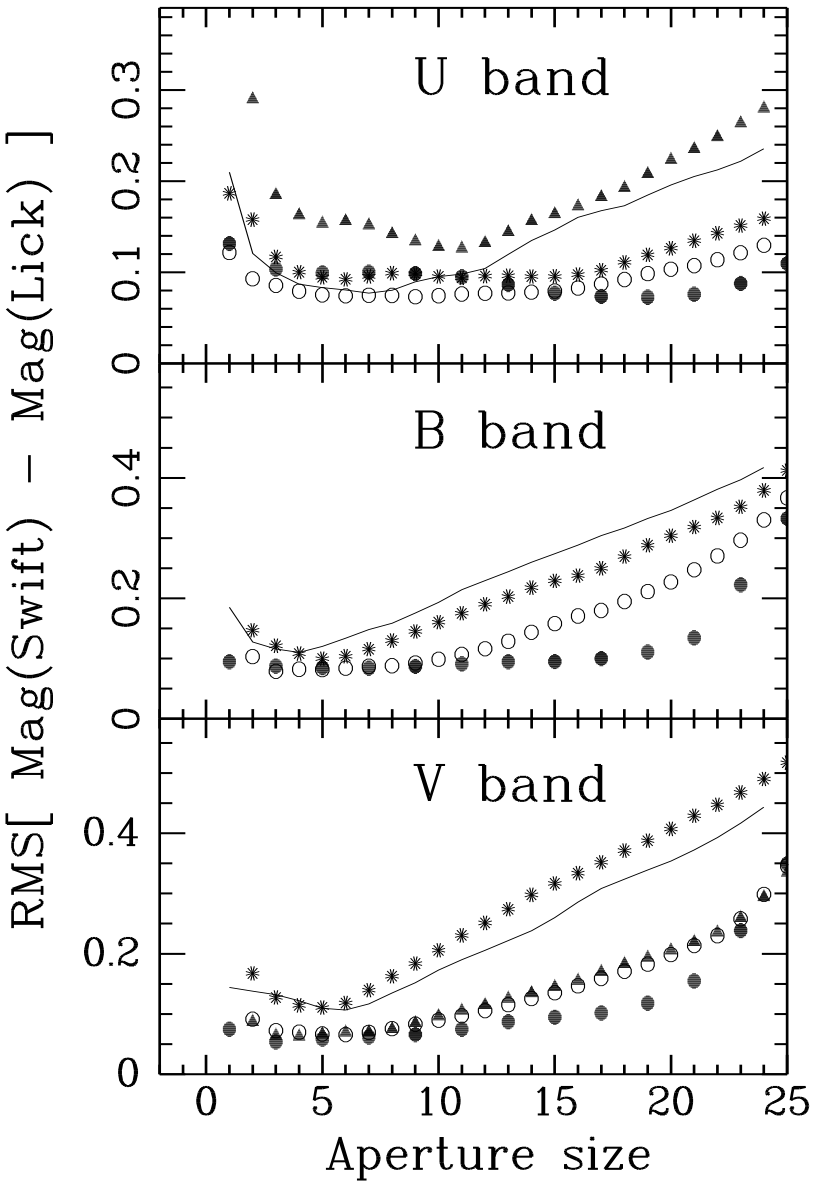

Fig. 6.— The RMS of the differences between the UVOT photometry and the Lick calibrations, as a function of aperture size. Obs1 is shown as open circles, obs2 as solid circles, obs3 as stars, obs4 as solid triangles, and obs5 as solid lines. For obs2, the apertures are displayed as APT(used)$\times 2 - 1$. The smallest RMS is achieved when an aperture radius of 5 pixels (3 pixels for 2×2 binned data) is used to do photometry for the B and V bands. The U-band RMS has a flat distribution for aperture sizes in the 5–11 pixel range.

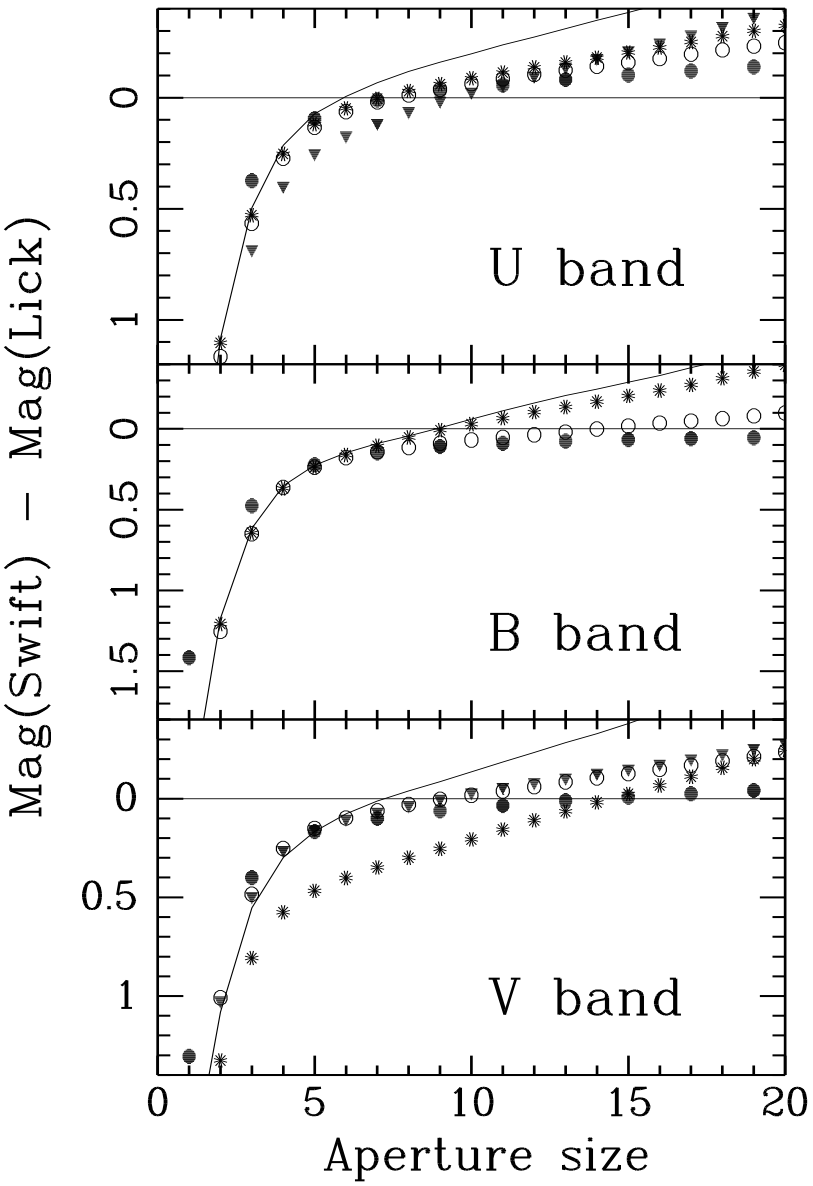

Fig. 7.— The difference between the UVOT photometry and the Lick calibrations, as a function of aperture size. The same symbols have been used as in Figure 6.

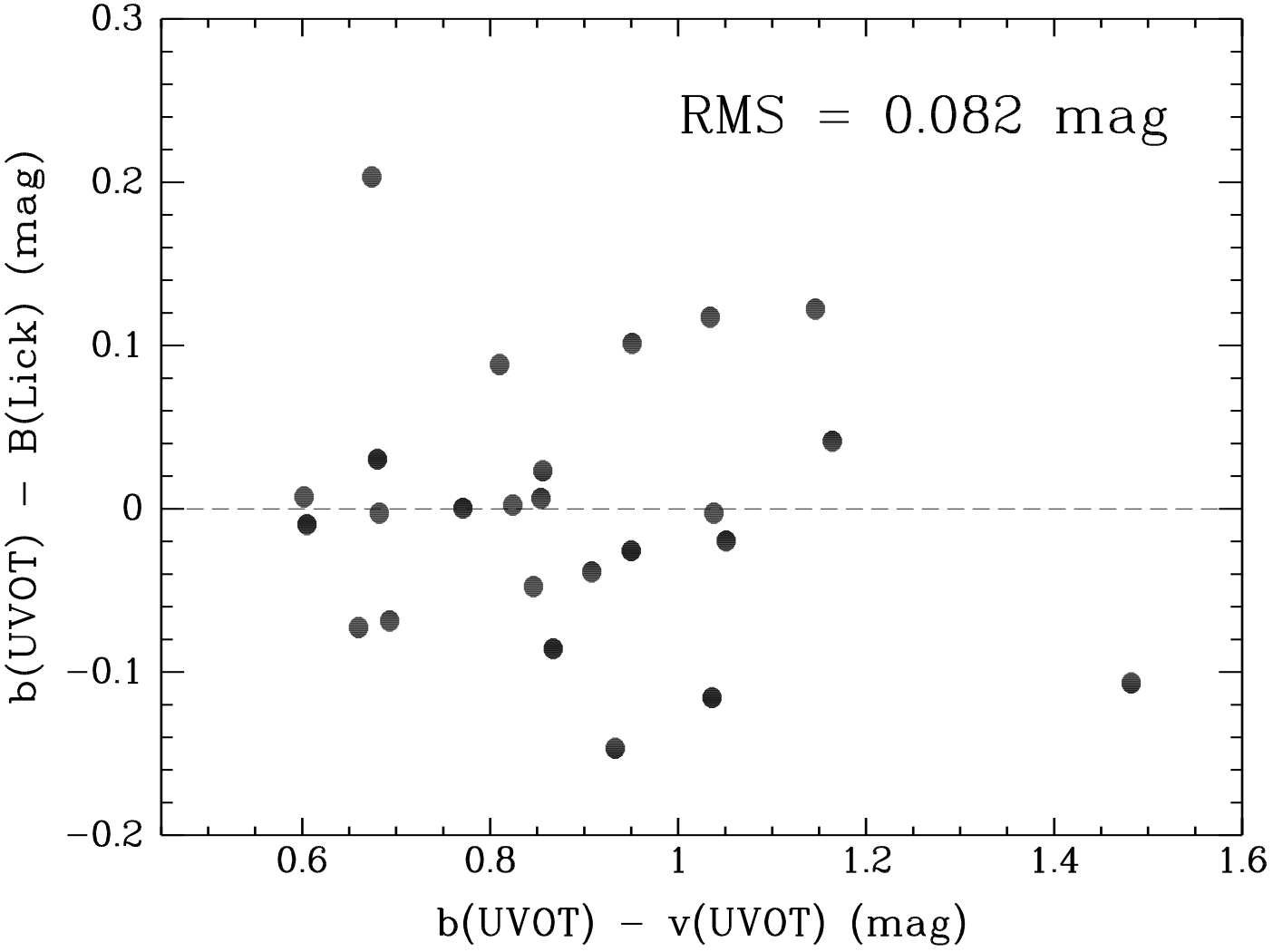

Fig. 8.— The residual $b(UVOT) - B(Lick)$ versus the $b(UVOT) - v(UVOT)$ color in obs1 B. The RMS is 0.082 mag, and there is no apparent correlation between the residuals and the colors.

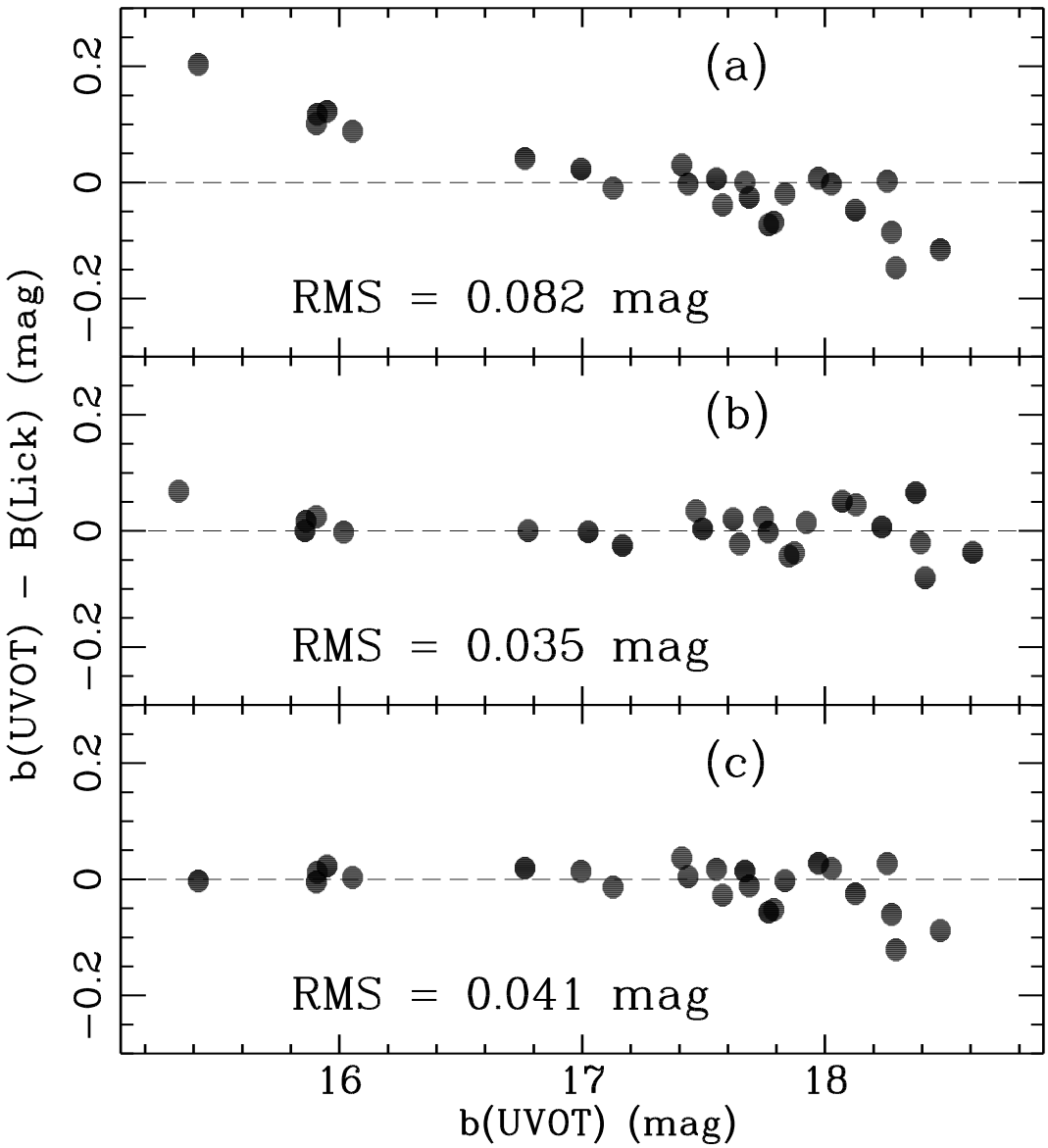

Fig. 9.— Panel (a): the residual $b(UVOT) - B(Lick)$ versus the magnitude $b(UVOT)$ in obs1 B, which shows a strong correlation. Panel (b): After a linear correlation is removed, the RMS is significantly improved. Panel (c): the residuals after coincidence-loss correction. No apparent correlation is present.

Fig. 10.— Finder charts for the fields near SN 2005cf. Both images were taken in the R band with the Nickel telescope on 2005 July 11 (field of view $6'.3 \times 6'.3$). The left panel includes SN 2005cf, while the right panel does not. Both panels are within the field of view for UVOT. North is up and east is to the left. SN 2005cf and the local standard stars listed in Table 7 are labeled.

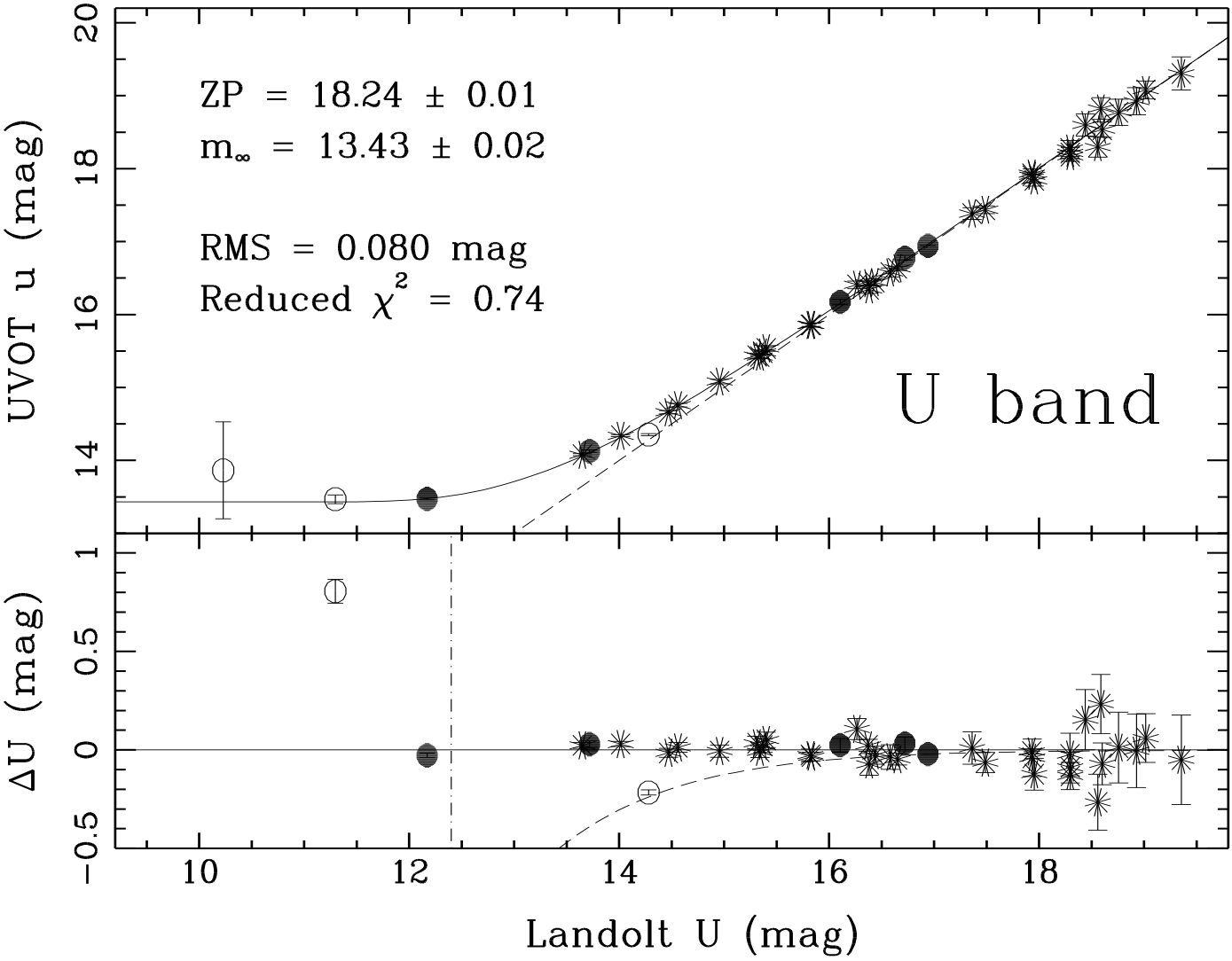

Fig. 11.— The coincidence-loss correction for the U band. The upper panel shows the Landolt U versus the UVOT u magnitudes for the Landolt standard stars (open circles) and the SN 2005cf field stars (stars). The solid line shows our model coincidence-loss correction, while the dashed line shows Landolt U = UVOT u. The open circles are the Landolt standard stars that are not used in fitting the coincidence-loss correction due to their extreme brightness or color. The lower panel shows the residuals of the fit. The dash-dotted line marks the Landolt U-band magnitude whose corresponding UVOT u-band magnitude is 0.1 mag fainter than m_∞.

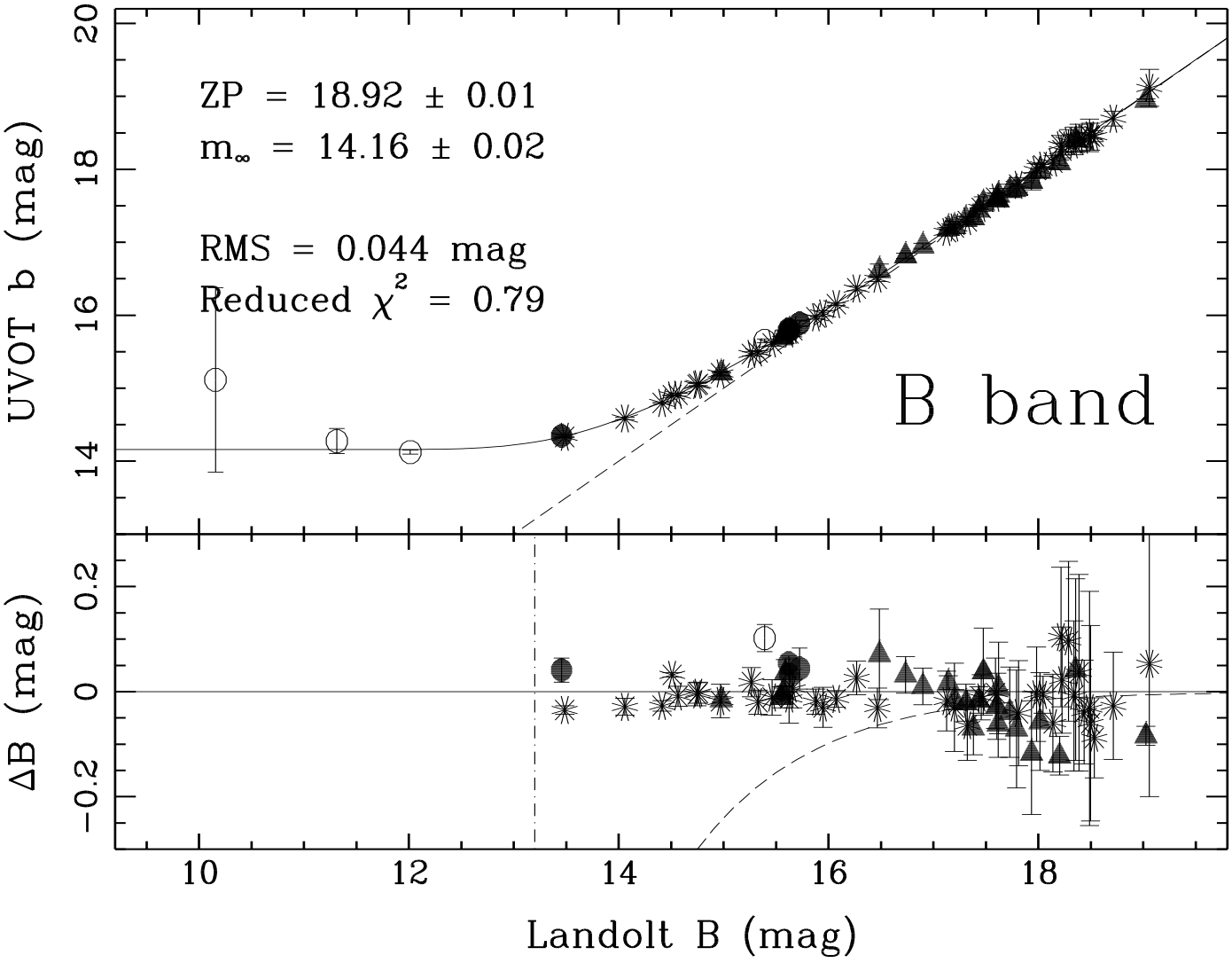

Fig. 12.— Same as Figure 11 but for the B band. The triangles are for the SN 2005am field stars.

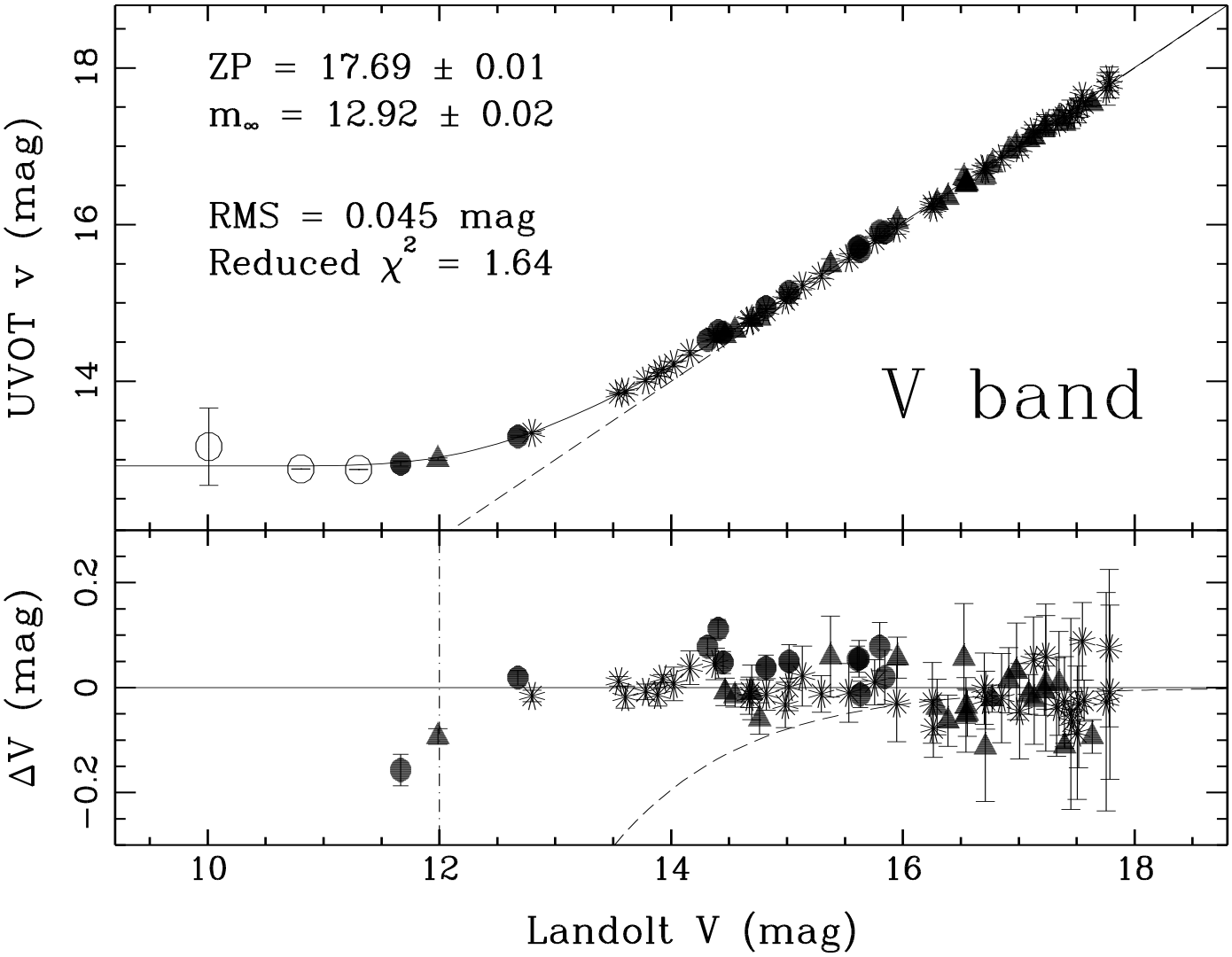

Fig. 13.— Same as Figure 11 but for the V band. The triangles are for the SN 2005am field stars.

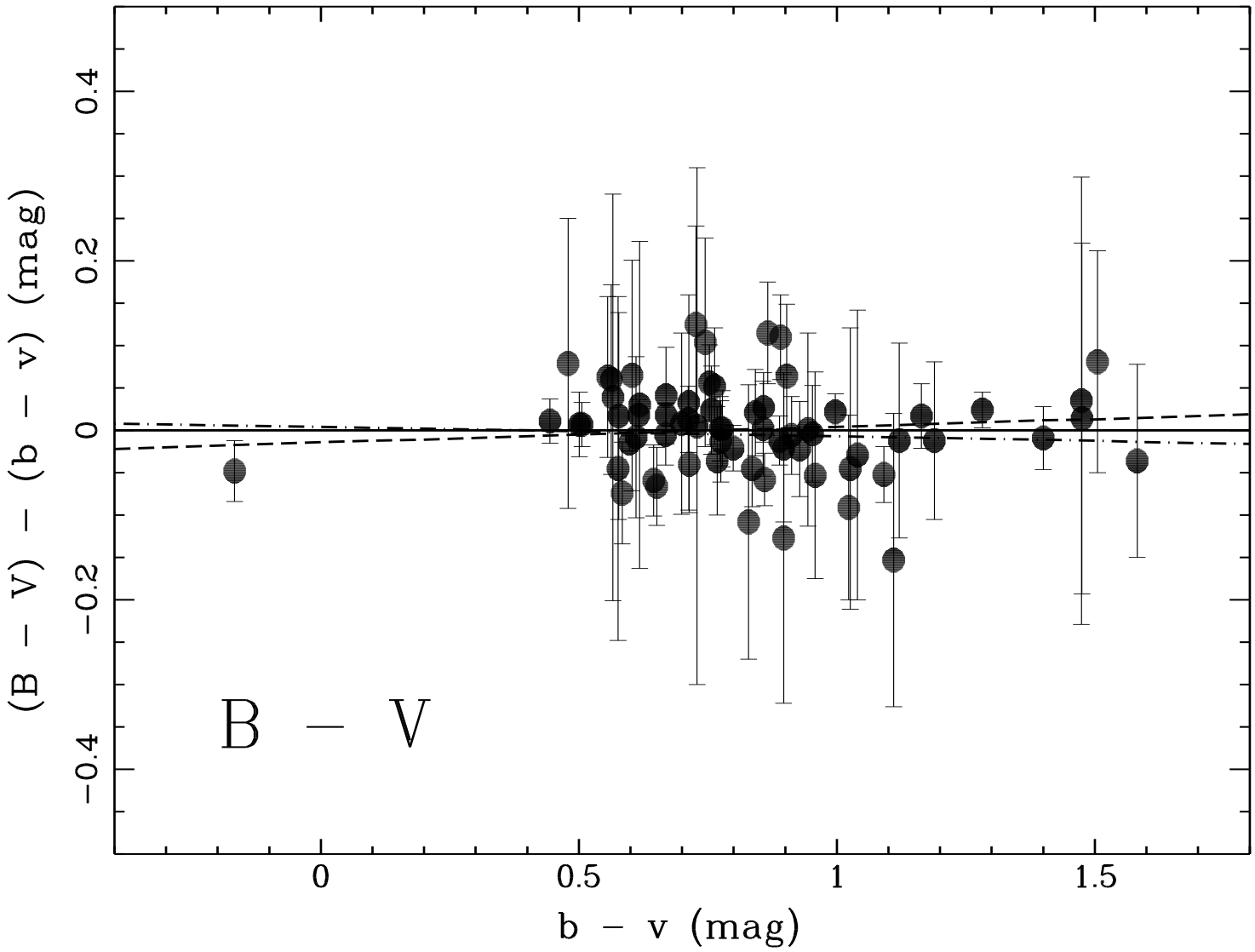

Fig. 14.— The difference between the $(B-V)$ and $(b-v)$ color, as a function of $(b-v)$. Also overplotted are three fitting functions: the solid line is $(B-V)=(b-v)$, the dash-dotted line is $(B-V)=0.004+0.989(b-v)$, while the dashed line is $(B-V)=-0.014+1.0184(b-v)$.

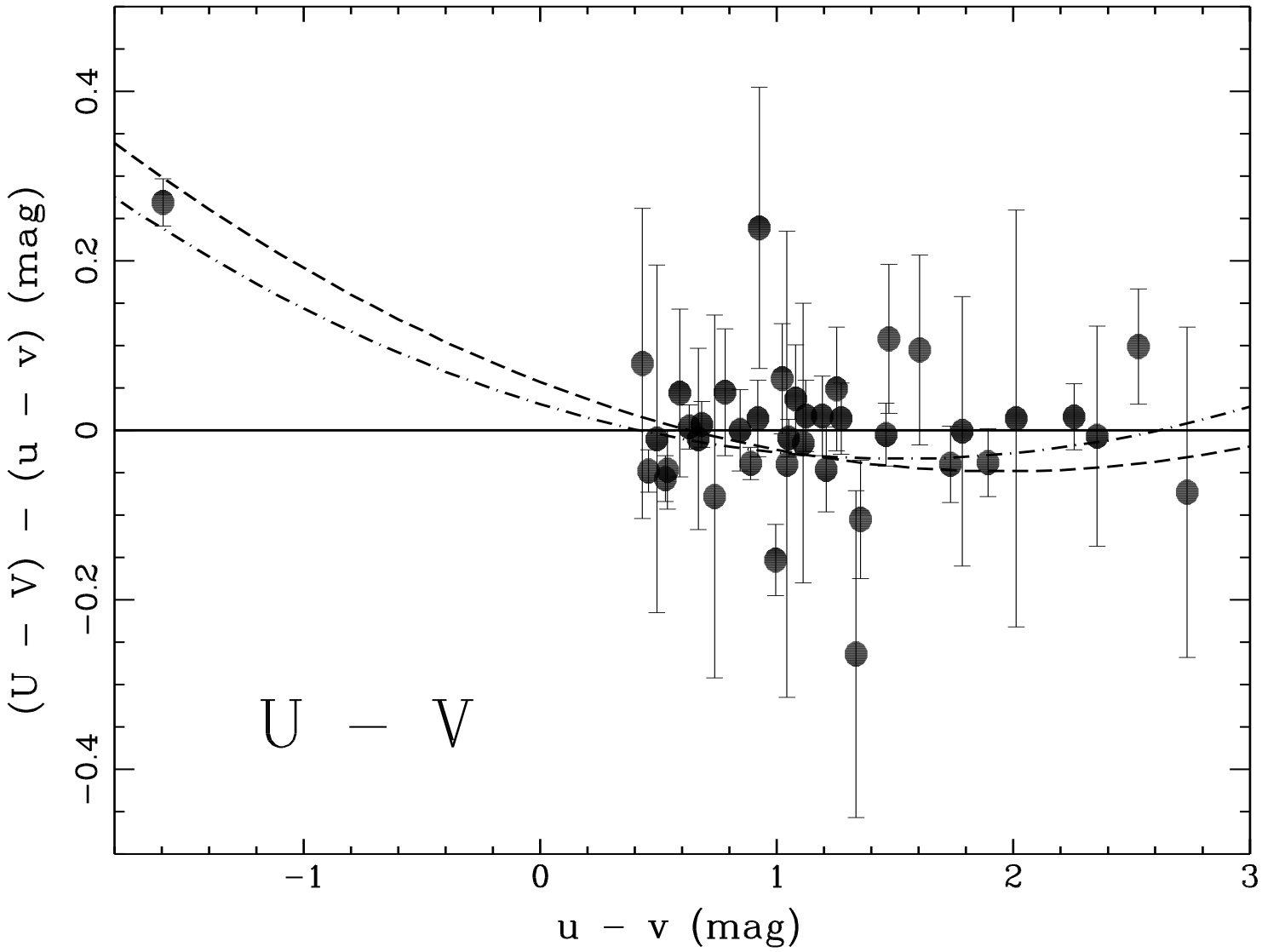

Fig. 15.— The difference between the $(U-V)$ and $(u-v)$ color, as a function of $(u-v)$. Also overplotted are three fitting functions: the solid line is $(U-V) = (u-v)$, the dash-dotted line is $(U-V) = 0.031 + 0.9150(u-v) + 0.028(u-v)^2$, while the dashed line is $(U-V) = 0.057 + 0.8926(u-v) + 0.0274(u-v)^2$.

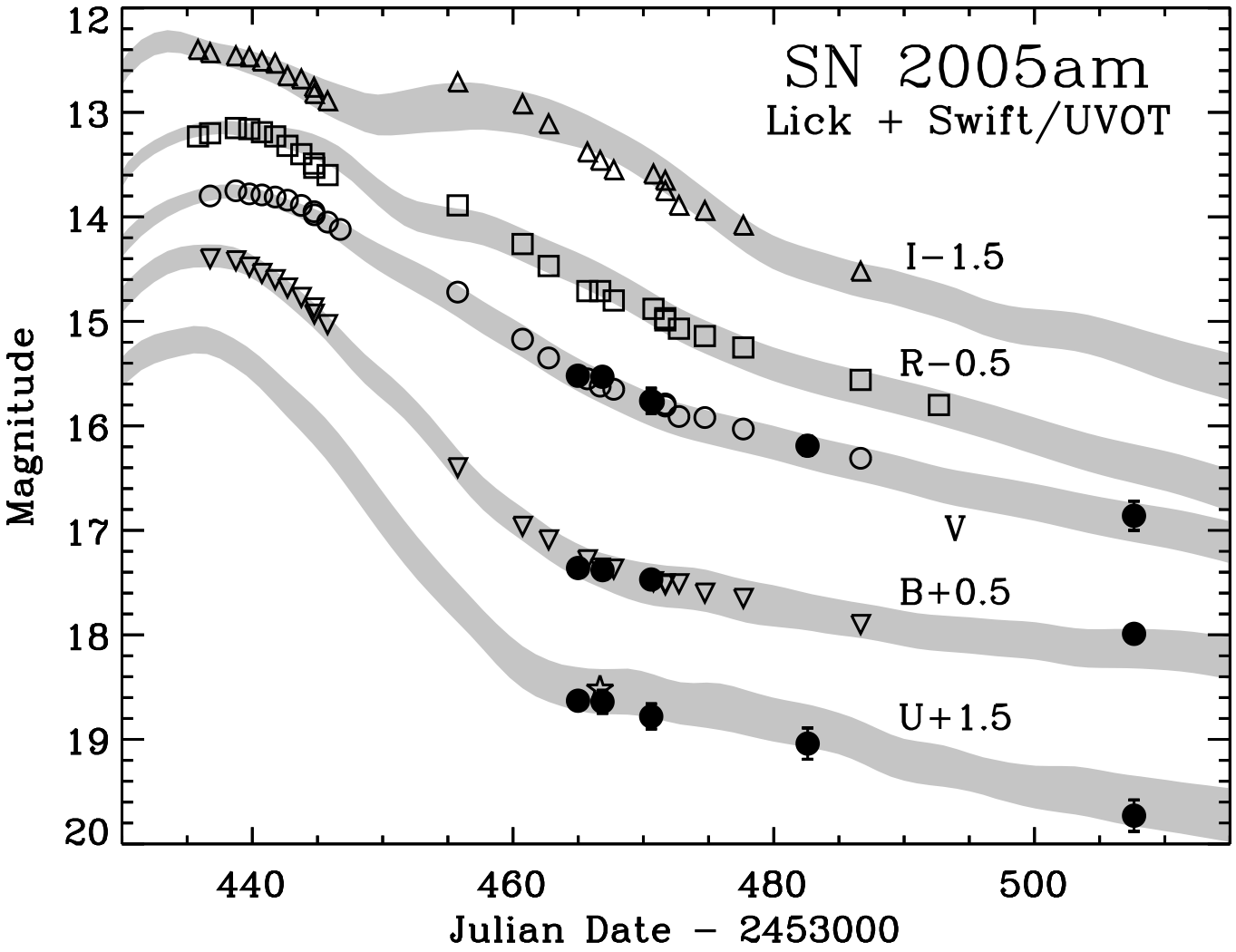

Fig. 16.— The ground-based (open symbols) and the UVOT (solid circles) photometry for SN 2005am. Also overplotted are the MLCS fits.

Fig. 17.— A finder chart ($6' \times 6'$) for the field of GRB 050603. This comes from a 2055.79 s UVOT V-band image that started at 01:25:45 on 2005 June 4. North is up and east is to the left. The optical afterglow (OA) and star S1 are labeled.

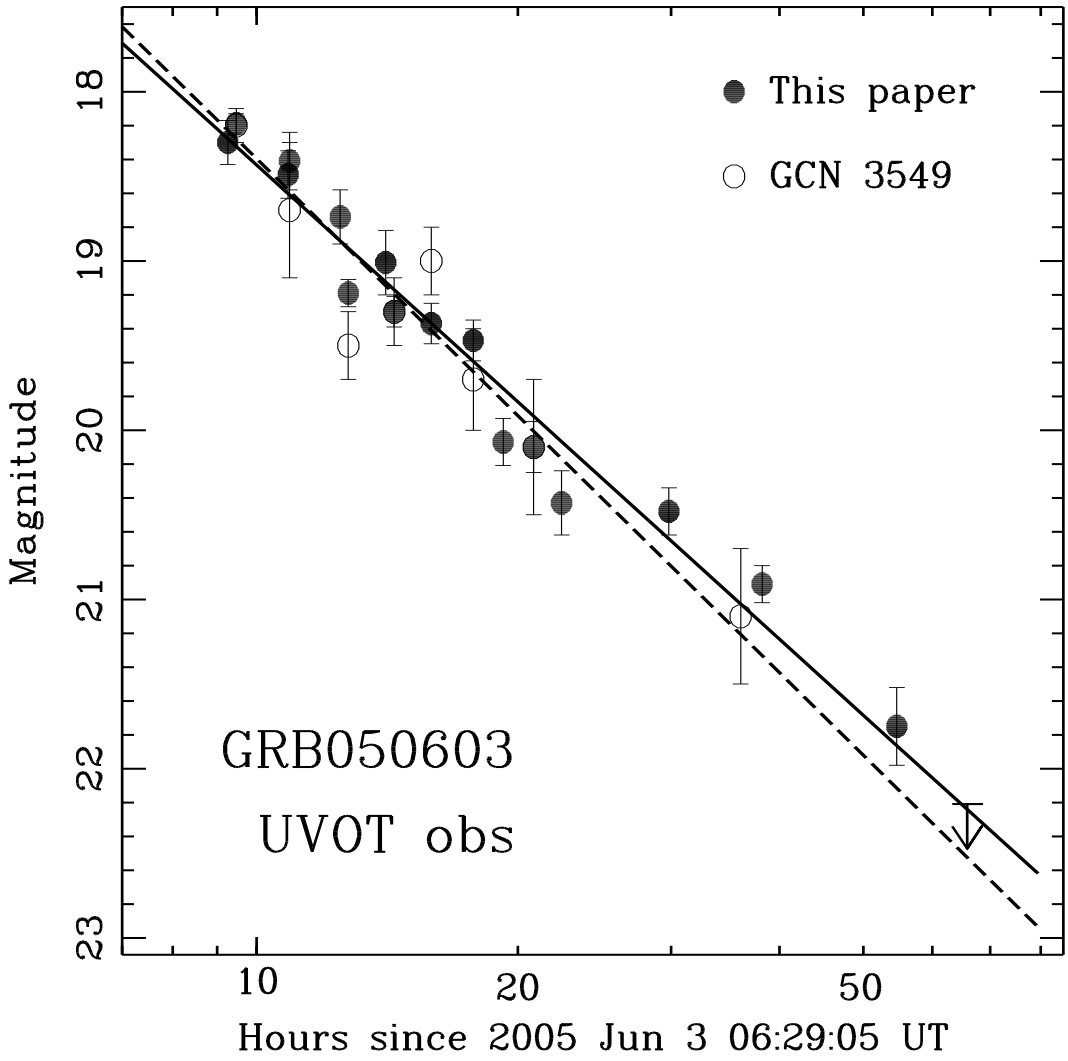

Fig. 18.— The UVOT V-band photometry for GRB 050603. The solid circles are from photometry reported in this paper, while the open circles are from GCN 3549 (Brown et al. 2005c). The solid line is a power-law fit to the solid circles, with $\alpha = -1.86 \pm 0.06$, while the dashed line is a power-law fit to the open circles, with $\alpha = -2.01 \pm 0.22$.

This figure "fig01.gif" is available in "gif" format from:

http://lanl.arXiv.org/ps/astro-ph/0505504

This figure "fig04.gif" is available in "gif" format from:
http://lanl.arXiv.org/ps/astro-ph/0505504

This figure "fig10.gif" is available in "gif" format from:
http://lanl.arXiv.org/ps/astro-ph/0505504

This figure "fig17.gif" is available in "gif" format from:
http://lanl.arXiv.org/ps/astro-ph/0505504